1980

Most probable magnetohydrostatic equilibria for tokamaks and reversed field pinches

John Joseph Ambrosiano
College of William & Mary - Arts & Sciences

INFORMATION TO USERS

This was produced from a copy of a document sent to us for microfilming. While the most advanced technological means to photograph and reproduce this document have been used, the quality is heavily dependent upon the quality of the material submitted.

The following explanation of techniques is provided to help you understand markings or notations which may appear on this reproduction.

1. The sign or "target" for pages apparently lacking from the document photographed is "Missing Page(s)". If it was possible to obtain the missing page(s) or section, they are spliced into the film along with adjacent pages. This may have necessitated cutting through an image and duplicating adjacent pages to assure you of complete continuity.

2. When an image on the film is obliterated with a round black mark it is an indication that the film inspector noticed either blurred copy because of movement during exposure, or duplicate copy. Unless we meant to delete copyrighted materials that should not have been filmed, you will find a good image of the page in the adjacent frame.

3. When a map, drawing or chart, etc., is part of the material being photographed the photographer has followed a definite method in "sectioning" the material. It is customary to begin filming at the upper left hand corner of a large sheet and to continue from left to right in equal sections with small overlaps. If necessary, sectioning is continued again—beginning below the first row and continuing on until complete.

4. For any illustrations that cannot be reproduced satisfactorily by xerography, photographic prints can be purchased at additional cost and tipped into your xerographic copy. Requests can be made to our Dissertations Customer Services Department.

5. Some pages in any document may have indistinct print. In all cases we have filmed the best available copy.

University Microfilms International

300 N. ZEEB ROAD, ANN ARBOR, MI 48106
18 BEDFORD ROW, LONDON WC1R 4EJ, ENGLAND

AMBROSIANO, JOHN JOSEPH

MOST PROBABLE MAGNETOHYDROSTATIC EQUILIBRIA FOR TOKAMAKS AND REVERSED FIELD PINCHES

The College of William and Mary in Virginia PH.D. 1980

MOST PROBABLE MAGNETOHYDROSTATIC EQUILIBRIA FOR TOKAMAKS AND REVERSED FIELD PINCHES

A Dissertation

Presented to

The Faculty of the Department of Physics

The College of William and Mary in Virginia

In Partial Fulfillment

of the Requirements for the Degree of

Doctor of Philosophy

---

by

John Ambrosiano

March 1980

APPROVAL SHEET

This dissertation is submitted in partial fulfillment of

the requirements for the degree of

Doctor of Philosophy

John Joseph Ambrosiano

Approved, March 1980

George M. Vahala

David C. Montgomery

Frederic R. Crownfield, Jr.

Edward A. Remler

Thomas A. Zang
Department of Mathematics

TABLE OF CONTENTS

ACKNOWLEDGMENTS

I wish to thank Dr. George Vahala for his continued guidance and encouragement, and for many helpful suggestions during the course of this work. I also wish to thank Drs. David Montgomery, Fred Crownfield, and William Matthaeus for their meaningful discussions and inquiring comments.

ABSTRACT

The determination of magnetohydrostatic equilibria usually requires that two of the equilibrium functions be given. As there is usually no a priori basis for specifying the form of these two functions, the functions and the equilibria they determine may be considered random.

In this dissertation, the author reviews a recent statistical method for determining the equilibrium of an axially symmetric cylindrical plasma which is most probable (in the maximum entropy sense) given four global constraints (i.e., energy, magnetic helicity, longitudinal magnetic flux, and longitudinal current flux). Previous results from this model have been limited to non-negative random equilibrium functions (B_z, J_z, where $\underset{\sim}{B}$ is the magnetic field and $\underset{\sim}{J}$ is the current density), and to analytically derived solutions of the determining equations in which one constraint (magnetic helicity) has been relaxed.

The present work extends these results to the fully constrained problem by presenting numerically computed solutions of the governing equations. Some of these solutions are specialized to values of the constraints appropriate to tokamaks. States which are approximately force-free ($\underset{\sim}{B} = \underset{\sim}{J} \times$ const.) are shown to exist as solutions to the most probable state equations.

A further extension of the model is attempted in order to alleviate the restriction to non-negative random equilibrium functions. The extended model is applied to the problem of finding most probable equilibria with reversed magnetic fields. An examination of solutions constrained to different values of energy and magnetic helicity shows a tendency toward low pressure equilibria when the energy-to-helicity ratio is lowered. This result is consistent with the Bessel function model of reverse-field equilibria in which dynamical relaxation of the energy with respect to a fixed magnetic helicity results in pressureless, Bessel function equilibria.

A study is made of the influence of the pinch ratio, and experimental parameter, on the degree of magnetic field reversal in the most probable state model. The dependence of solutions on this parameter is found to be consistent qualitatively with experiments.

FIGURES

MOST PROBABLE MAGNETOHYDROSTATIC EQUILIBRIA FOR TOKAMAKS AND REVERSED FIELD PINCHES

I. INTRODUCTION

The theoretical study of magnetohydrodynamic (MHD) equilibria has gone on since the early days of plasma physics. Yet, it has not been until the recent efforts to produce controlled thermonuclear reactions (beginning in the United States with Project Sherwood[1] in 1952) that the subject has received so much attention. It is because of the densities, time scales and geometries of interest in fusion research that such importance has been attributed to ideal MHD equilibria and their stability properties.

For the parameters of interest in magnetic fusion research, involving particle number densities of $\gtrsim 10^{14}$ cm^{-3}, kinetic temperatures on the order of 10 keV, and confinement time scales less than one second, binary collisions between particles are relatively unimportant in determining the plasma properties. In such time, a plasma will not relax to a state of thermal equilibrium, yet because of the long range Coulomb force, collective effects in the plasma can produce changes in the configurations on a much shorter time scale ($\sim$1 μs). In this regime, the steady state solutions of the macroscopic fluid equations characterize possible plasma equilibria. One may regard these solutions as metaequilibria since, in general, they do not represent states of thermodynamic equilibrium.

To study the tendency of such configurations to persist on the brief confinement time scales, one traditionally employs a perturbation analysis.[2] After a steady state solution is found, the effects of small perturbations on the equilibrium are studied by means of the linearized equations of motion. If the initial perturbation grows, the plasma is termed unstable. This kind of analysis is often applied to the ideal MHD equations, because of the relative ease with which they can be applied to boundary value problems in fusion related geometries.

In many plasma experiments an equilibrium state is never established, because the time required to produce the plasma is comparable to the growth time of an instability. In such cases, the role of the theoretician has often been to make conjectures about how some model equilibrium configuration might have been attained if the instabilities had been suppressed. The experimentalist may in turn attempt to determine the operating parameters that might lead to the establishment of such a configuration.

This interaction between theory and experiment has been considerably successful in eliminating the most dangerous macroscopic instabilities. Yet the cooperation between the two disciplines is often complicated by the lack of detailed information. The solution of the steady state equations for ideal MHD usually requires the arbitrary specification of two equilibrium functions. The theoretician must somehow make a choice for these functions compatible with experimental

data. Such data, however, is often insufficient for a complete determination of the functions. The experimentalist, on the other hand, works in parameter regimes characterized by certain global constraints such as the toroidal flux and toroidal current. The difficulty of obtaining information about detailed configurations of the system from experimental diagnostics, usually limits the ability of the experimentalist to manipulate the plasma in the direction of some desired equilibrium configuration.

Recently, Montgomery, Turner, and Vahala[3] proposed a statistical procedure for determining the "most probable" equilibrium compatible with certain global constraints. Two free equilibrium functions were treated as random entities, a discrete representation of the field was employed to characterize all possible choices, and then an a priori probability was assigned to the realization of any one state. Subsequent maximization of the probability then yielded equations for the most probable state compatible with the constraints imposed.

This approach is analogous to the Boltzmann method[4] of deriving the canonical distribution by maximizing the a priori probability associated with the realizations of a particular macroscopic configuration of point particles. The technique also has some aspects in common with the methods of information theory, developed by Shannon,[5] in which an unknown probability distribution is inferred by maximizing, subject to available information, the "uncertainty" associated with the distribution.

In this dissertation, we will examine solutions of the equations derived by Montgomery, et al.[3] In particular, most probable equilibria will be found for two important types of toroidal pinch: the tokamak and the reverse-field pinch. In the latter case, an extension of the method (also suggested by Montgomery)[6] is required.

A. Ideal Magnetohydrodynamics

The conventional means of investigating the stability of plasma configurations has been through the ideal magnetohydrodynamic (MHD) model, even though ideal MHD describes no real plasma.[7]

The ideal MHD equations are extensions of the hydrodynamic equations to perfectly conducting fluids. The basic relations include an equation for conservation of mass,

$$\frac{\partial \rho}{\partial t} + \nabla \cdot (\rho \underset{\sim}{v}) = 0 \tag{1}$$

where ρ is the mass density and $\underset{\sim}{v}$ the fluid velocity, and conservation of momentum

$$\frac{D\underset{\sim}{v}}{Dt} = -\nabla p + \underset{\sim}{J} \times \underset{\sim}{B} \tag{2}$$

where D/Dt is the convective time derivative $\frac{\partial}{\partial t} + \underset{\sim}{u} \cdot \nabla$ which follows the fluid element, p is the scalar preasure, $\underset{\sim}{J}$ is the current density, and $\underset{\sim}{B}$ the magnetic induction. For consistency,[8] the displacement current is dropped from Maxwell's equations

$$\nabla \times \underset{\sim}{E} = -\frac{\partial \underset{\sim}{B}}{\partial t} \tag{3}$$

$$\nabla \times \underset{\sim}{B} = \mu_o \underset{\sim}{J} \tag{4}$$

A restricton of the model to low frequency phenomena is implied by the absence of the displacement current in Eq. (4). The electric field is eliminated by use of Ohm's law for a perfectly conducting fluid.

$$\underset{\sim}{E} = \underset{\sim}{u} \times \underset{\sim}{B} \tag{5}$$

The fluid is also assumed to behave in such a way as to remain charge neutral, so that $\underset{\sim}{J}$ and $\underset{\sim}{B}$ are both solenoidal fields, i.e.,

$$\nabla \cdot \underset{\sim}{J} = 0; \quad \nabla \cdot \underset{\sim}{B} = 0 \tag{6}$$

Finally, to close the system of equations, an equation of state is required:

$$\frac{DS}{Dt}(p,\rho) = 0 \tag{7}$$

where S is the thermodynamic entropy per unit volume.

Ideal MHD, being a fluid description, is in principle only appropriate where collisions force the particles to move together as a fluid element. Yet in many experiments the mean-free-path for collisions is often comparable to the dimensions of the apparatus. Even when collisions are rare, a fluid description can be justified if the magnetic fields are sufficiently strong. The particles are then closely tied to magnetic field lines, and the plasma may behave as a fluid in the transverse direction. However, particles are free to stream along the field lines in this case. This is the approach of the Guiding Center Plasma model[9] (G.C.P.) which describes the plasma by a kinetic (Vlasov) equation along the field lines and fluid equations (conservation laws) in the transverse direction. The assumption of a scalar pressure in ideal (MHD) is sometimes considered to be too strong, particularly in the presence of strong magnetic fields. Theories like the Double Adiabatic Theory [10] and the GCP model, both of which admit anisotropies in the pressure tensor are more appropriate than ideal MHD in such instances.

Yet in spite of the fact that very often the use of ideal MHD cannot be physically justified, and that more realistic models are available, ideal MHD is the most widely used description in assessing the stability of plasma configurations. There are several important reasons underlying this choice. First of all, ideal MHD is the simplest model. In complicated geometries of interest in fusion research, this simplicity is all important. Secondly, with

respect to linear stability criteria, ideal MHD stability is often sufficient for the stability of other more realistic (and more complicated) models.[2] Finally, the mathematical properties of the ideal MHD equations are well understood. This leads to a large number of mathematically well-posed problems.

B. Magnetohydrostatic Equilibria and the Grad-Shafranov Equation[11,12]

Much theoretical effort has been devoted to the identification of static ideal MHD equilibria. These are configurations in which there is no gross fluid motion ($\underset{\sim}{v} = 0$) and where the force on a fluid element ($\underset{\sim}{J} \times \underset{\sim}{B}$) is exactly balanced by the pressure gradient. The equations which determine the equilibria are

$$\nabla p = \underset{\sim}{J} \times \underset{\sim}{B} \tag{8}$$

with

$$\mu_o \underset{\sim}{J} = \nabla \times \underset{\sim}{B} \tag{9}$$

and

$$\nabla \cdot \underset{\sim}{B} = 0 \tag{10}$$

Mathematical properties of this system may be investigated by the method of characteristics. A characteristic is a surface or manifold across which the normal derivatives of the function cannot be computed. Characteristic surfaces can thus be pictures as wavefronts because of

this discontinuity. If all characteristic surfaces are real, the system of partial differential equations is called hyperbolic; if all the surfaces are complex, the system is called elliptic. When the system fits one of these categories, theorems become available to indicate the conditions under which the problem is well-posed. When the system does not fit one of the two categories, general theorems concerning well-posedness are not available and solutions may not be guaranteed under arbitrary conditons. An examination of equations (8)-(10) shows that this 4th order system is of a mixed type, with two real and two complex characteristic surfaces. However, if at least one coordinate is ignorable, the symmetry allows the system to be reduced to one of the standard elliptic type. The hyperbolic part is effectively integrated out giving rise to two free functions.

As an example of how these arbitrary functions arise in the problem of determining MHD equilibria, consider the equilibrium of a straight cylindrical plasma in which the θ-coordinate is ignorable. Because of the symmetry, Eq. (10) leads to the existence of a stream function ψ such that

$$\underset{\sim}{B} = \frac{1}{r}\frac{\partial \psi}{\partial Z}\,\hat{r} + B_\theta \hat{\theta} - \frac{1}{r}\frac{\partial \psi}{\partial r}\,\hat{Z} \tag{11}$$

The current density is therefore

$$\underset{\sim}{J} = \nabla \times \underset{\sim}{B} = -\frac{1}{r}\ \Delta^{*}\psi\hat{\theta} + \nabla(rB_{\theta}) \times \nabla\theta \tag{12}$$

where Δ^{*} is an elliptic operator defined by

$$\Delta^{*}\psi \equiv r\frac{\partial}{\partial r}\left(\frac{1}{r}\frac{\partial\psi}{\partial r}\right) + \frac{\partial^{2}\psi}{\partial Z^{2}} \tag{13}$$

The function ψ is usually interpreted as a coordinate in which the values ψ = const. label a set of simply nested cylinders, and where the value of ψ on the surface of one of these cylinders is proportional to the magnetic flux through its cross section. Magnetic field lines lie entirely on these surfaces since

$$\underset{\sim}{B} \cdot \nabla\psi = 0 \tag{14}$$

Hence they are called magnetic surfaces.

Because

$$\underset{\sim}{B} \cdot \nabla p = \underset{\sim}{B} \cdot \underset{\sim}{J} \times \underset{\sim}{B} = 0 \tag{15}$$

the pressure is also a surface quantity, i.e.,

$$p = p(\psi) \tag{16}$$

Taking this dependence into account, the pressure balance equation (8) thus becomes

$$\begin{aligned} p'(\psi)\nabla\psi &= \underset{\sim}{J} \times \underset{\sim}{B} \\ &= \frac{-1}{r^{2}}\,(\Delta^{*}\psi)\nabla\psi \\ &\quad -r\,\frac{B_{\theta}}{r^{2}}\,\nabla(rB_{\theta}) \end{aligned} \tag{17}$$

Rewriting Eq. (17) as

$$\left[p'(\psi) + \frac{1}{r^2} \quad (\Delta^* \psi)\right] \nabla\psi = -r \frac{B_\theta}{r^2} \nabla (rB_\theta) \tag{18}$$

it becomes evident that rB_θ is also a function of ψ, i.e., $rB_\theta \equiv \chi(\psi)$ is a surface quantity, and hence Eq. (18) may be written as

$$\Delta^* \psi = -r^2 p'(\psi) + \chi\chi'(\psi) \tag{19}$$

Equation (19) is one form of the Grad-Shafranov equation.[11,12] Its solution can be found if one specifies the two functions of ψ appearing in the inhomogeneous term on the right hand side, together with appropriate boundary conditions on an elliptic partial differential equation.

Thus one finds that, in the presence of a symmetry, the solution of the reduced equilibrium equation requires the specification of two arbitrary functions. In general, any two independent equilibrium functions may be regarded as arbitrary. The subsequent determination of the equilibrium is then dependent on the assumed form of these two functions.

C. Tokamaks and Reverse-Field Pinches

A controlled fusion device must satisfy certain basic requirements. If one uses deuterium and tritium as fuel for the reaction

$$D + T \rightarrow {}^4He + n \qquad (20)$$

kinetic temperatures of 10 keV or more must be achieved. At this temperature the constituents would be in a plasma state. It was Lawson[13] who developed a criterion by which a plasma of density n confined for a time τ produces thermonuclear energy in excess of the energy required to initiate the reactions. This value is $n\tau \sim 10^{14}$ cm^{-3} sec. Since plasmas are composed of charged particles, confinement by appropriate magnetic field and current configurations is possible. To the degree that plasma behavior can be predicted by the ideal MHD model, a considerable amount of effort has been devoted to the task of finding ideal MHD equilibria which are stable. In this context the word "stability" implies that the worst instabilities predicted by the linearized MHD equations should have e-folding times which are large compared with the desired confinement time.[14] The ultimate aim of the fusion program is of course to produce economical power. Hence the cost of achieving a stable magnetic confinement is also important. One rule-of-thumb estimate of the cost of magnetic confinement schemes is found in the plasma parameter beta. Roughly speaking a plasma equilibrium is attained by balancing the kinetic pressure $p = nkT$ against the magnetic pressure $1/2\ B_c^2$. The ratio

$$\beta_{pl} = 2p / B_c^2 \qquad (21)$$

gives a rough measure of how effectively the magnetic field is used.

(The subscript pl will be used throughout to avoid confusion with another parameter beta which appears later in a different context.) Ideally $\beta_{pl} = 1$. If β_{pl} is small, then much more magenetic field strength is generated than ought to be required for equilibrium. Since magnetic fields are a substantial part of the expense of building magnetic confinement devices, a low β_{pl} device is less desirable than one of higher β_{pl}. In practical terms the design of any device is a tradeoff among the parameters of an ideal system. What follows is a brief description of two devices belonging to the toroidal pinch category. These two types - the tokamak, and the reversed-field pinch - operate in opposite parameter regimes. Each has certain advantages and disadvantages and both are serious candidates in the search for a fusion reactor.

The tokamak is a device based upon the idea of confining a plasma to a toroidal region by producing a very strong magnetic field in the toroidal direction (the long way around the torus). This is done by means of current carrying coils wrapped poloidally (the short way) around the torus. The strongly magnetized particles would in principle be tied to the magnetic lines of force thereby preventing them from contacting the walls of the toroidal shell. This simple idea, however, has a serious problem arising from the toroidal geometry itself. Such a configuration has an inevitable gradient in the direction of the major axis (as may be easily verified by Ampere's Law). This gradient produces particle drifts which rapidly destroy

confinement. The remedy is to twist the field lines into a helical shape by the addition of a poloidal component B_p in the torus. In the design of tokamaks this component is produced by a toroidal current which itself is induced by a transformer effect in which the plasma is the one-turn secondary coil. The toroidal current also serves to heat the plasma ohmically. Only a small B_p component is required so that typically, $B_T \gg B_p$, where B_T is the toroidal field. With this ordering Kruskal[15] and Shafranov, using an idealized model, were able to predict the limit of stable operation for a tokamak in terms of a parameter q(r), defined by

$$q(r) \equiv \frac{r}{R} \frac{B_T(r)}{B_p(r)} \tag{22}$$

where r is the distance from the minor axis and R is the major radius. The stability condition is

$$q > 1 \tag{23}$$

In the usual terminology q is called the "safety factor". Other stability considerations,[16] combined with this basic condition, require that

$$q(a) = \frac{2\pi}{\mu_o} \frac{B_T}{R} \frac{a^2}{I} \gtrsim 2.5 \tag{24}$$

where a is the minor radius and I is the toroidal current. From this one sees that, for a given toroidal field, the current in a stable tokamak is limited by the safety factor. Limitations on current prevent the tokamak from reaching ignition temperature by ohmic heating alone. Another problem stems from the fact that, in

a tokamak, the plasma pressure is balanced mainly by the poloidal field so that β_{pl} is a small number on the order of a few % at best. Nevertheless, tokamak discharges are easily reproducible and fairly long lived, with energy confinement times of many milliseconds. There are also indications that auxilliary heating by means of neutral particle beams may be able to produce the required temperature, while increasing β_{pl} as a result of the rapid increase in pressure.

The reversed-field pinch is easiest to conceive as a modification of the stabilized Z-pinch. The linear Z-pinch[17] is one of the simplest concepts of confinement by self-pinching. Consider a cylindrical plasma through which a longitudinal current is passed. The resultant B_θ field interacts with the current, through the $\underset{\sim}{J} \times \underset{\sim}{B}$ force, to drive the plasma inward. Unfortunately, this simple scheme is macroscopically unstable to small perturbations of the plasma column. Any perturbation which makes the plasma surface concave, produces a locally intensified magnetic field which acts back on the plasma to increase the perturbation. These are the famous "sausage" and "kink" instabilities, so called because of the appearance of the deformed plasma. Linear stability analyses in ideal MHD predict a stabilization of such perturbations if a B_z component ($B_z \sim B_\theta$) is added. These predictions, (supported by experiments), led to the development of the stabilized Z-pinch of which there are toroidal versions to counteract endloss. In this regime stability depends on the detailed shapes of B_z and B_θ as

functions of the minor radius. The field lines, being helical, are characterized by the pitch of the helix as a function of r. The pitch is given by

$$\mu(r) = \frac{B_\theta(r)}{rB_z(r)} \tag{25}$$

and stability is generally enhanced in this parameter regime if its derivative $d\mu/dr$, called the shear, is large. One way to attain very high shear is by choosing a B_z profile which changes sign near the edge of the plasma; i.e. a reversed field. Based upon linear stability analyses is believed that reversed-field pinches may be stable at $\beta_{pl} \sim 30 - 40\%$ whereas a stabilized Z-pinch (without reversal) can only achieve $\beta_{pl} \sim 5\%$.[18] Limitations on the current are not as severe as in the tokamak, leading to the belief that a reverse-field pinch could reach ignition soley by ohmic heating.[18] Setting up the proper fields is a difficult task which is accomplished in one of two ways. The first method is a fast programming of the fields by external circuitry - a process which can be modeled numerically. The second is self-reversal - a phenomenon believed to involve turbulence. Confinement times in reverse-field pinches ($\sim \mu s$) are presently less than those for a tokamak. A dimensionless parameter of recurring interest in the reversed-field pinch literature is the pinch ratio Θ (analogous to the safety factor of the tokamak) given by

$$\Theta(r) = \frac{\mu_o r\, I}{2\Phi(r)} \tag{26}$$

where $\Phi(r)$ is the magnetic flux

$$\Phi(r) = \int_0^r B_z(\acute{r})\acute{r}d\acute{r} \quad . \tag{27}$$

Reversed fields are usually observed when $\Theta(a) \gtrsim 1.2$. Comparing the parameters that characterize tokamaks and reversed-field pinches one may note that a tokamak discharge must have $q(a) \gtrsim 2.5$ and typically $\Theta(a) < 1$. The reversed-field pinch on the other hand operates well below the Kruskal-Shafranov limit with $q(a) < 1$ and with $\Theta(a) \gtrsim 1.2$. The tokamak and the reversed-field pinch are, in a sense, devices which are in opposite parameter regimes.

D. Taylor's Theory of Relaxed Toroidal Discharges

A remarkable aspect of toroidal discharges is their tendency, in many cases, to evolve toward a quiescent state after an initially violent period. These final states are more or less independent of the initial configuration and seem instead to depend on a few global parameters. An example is the spontaneous reversal of the toroidal magnetic field component observed to occur in the large stabilized Z-pinch called ZETA.[18]

A theory to explain this sort of evolution (with particular emphasis on self-reversal) was advanced by Taylor.[19] Taylor conjectured

that the final configuration must represent some minimum energy configuration towards which the plasma must relax, subject to whatever constraints are imposed on the system. If the internal plasma energy is taken to be small relative to the magnetic field energy, one must seek a minimum of the energy integral $E = 1/2 \int B^2 \, dv$, subject to certain constraints. The problem then becomes one of identifying the relevant constraints.

It is well known that the magnetic lines of force in a perfectly conducting fluid are "frozen in". That is to say the fluid motion cannot change the field line topology. This constraint can be expressed in terms of the integral invariant

$$H_\alpha = \int_\alpha \underset{\sim}{A} \cdot \underset{\sim}{B} \, dv \tag{28}$$

Here, $\underset{\sim}{A}$ is the magnetic vector potential and the integral is taken over the volume of a tube bounded by magnetic field lines. There are an infinite number of such constraints; one for each tube of flux. It was Taylor's assumption that, in the presence of small but non-zero resistivity (where now topological changes can occur in the field lines because of the resistive effects), only one of these constraints remains; namely the integral over the entire plasma, assumed to be bounded by a conducting wall. Thus the quantity

$$H = \int_V \underset{\sim}{A} \cdot \underset{\sim}{B} \, dv \tag{29}$$

called the magnetic helicity, was taken to be an invariant during the evolution of the discharge. A minimum energy state subject to a fixed magnetic helicity is easily found by the method of Lagrange multipliers. One sets to zero the variation

$$\delta \int_V dv \left[\frac{1}{2} \underset{\sim}{B}^2 - \frac{\lambda}{2} \underset{\sim}{A} \cdot \underset{\sim}{B} \right] \tag{30}$$

and using the identity for any vector $\underset{\sim}{F}$,

$$\nabla \times \delta \underset{\sim}{A} \cdot \underset{\sim}{F} = \delta \underset{\sim}{A} \cdot (\nabla \times \underset{\sim}{F}) - \nabla \cdot (\underset{\sim}{F} \times \delta \underset{\sim}{A}) \tag{31}$$

obtains

$$\int_V dv \; \delta \underset{\sim}{A} \cdot \left[\nabla \times \underset{\sim}{B} - \lambda \underset{\sim}{B} \right] -$$

$$\int_V dv \; \nabla \cdot \left[\delta \underset{\sim}{A} \times (\underset{\sim}{B} - \frac{\lambda}{2} \underset{\sim}{A}) \right] = 0 \tag{32}$$

The second integral vanishes by the divergence theorem and the assumption of a fixed boundary with respect to variations of $\underset{\sim}{A}$. Thus

$$\nabla \times \underset{\sim}{B} = \lambda \underset{\sim}{B} = \mu_o \underset{\sim}{J} \tag{33}$$

indicating that the minimum energy state is force-free.

Assuming the relaxed state to be a function only of r, a Bessel function solution

$$B_r = 0 \tag{34}$$

$$B = B_o J_o(\lambda r) \tag{35}$$

$$B_\theta = B_o J_1(\lambda r) \tag{36}$$

is found immediately. Since the boundary condition $(\underset{\sim}{B} \cdot \hat{r})_{r=a} = 0$ is trivially satisfied, λ must be determined from external conditions. A relation between the pinch ratio Θ and the eigenvalue λ is found by integration of B_z and J_z; thus

$$\Theta = \lambda a/2 \tag{37}$$

Since the first zero of J_o occurs at $\lambda a = 2.4$, the critical value of Θ for reversal is $\Theta = 1.2$, which is in fairly good agreement with experimental measurements.

The theory of Taylor shows, in some ways, remarkable agreement with experiments performed on ZETA and other reversed-field pinch experiments. It is an encouraging example of a method which provides useful predictions from the knowledge of a few global quantities. There are certain features of the model, however, which do not agree with the experiments. The presaureless force-free states are usually not observed, but rather states of finite pressure are seen.

Values of magnetic helicity constructed indirectly from field probe measurements in the HBTX-1 device show a decay of helicity with time.[20] Therefore the timescale over which it is

appropriate to regard the helicity as fixed is uncertain. Finally, the reversal of the J_z current profile demanded by the force-free relation ($\underset{\sim}{J} = \lambda\underset{\sim}{B}$) when B_z is reversed, is not observed. That is, $J_z(r)$ is most often seen to be a non-negative function.

The most probable state model of the reversed-field equilibrium, to be presented in Chapter II, is different from the Bessel function model in certain important respects which must be emphasized. First of all Taylor's theory is a dynamical theory based upon the relaxation of the system to a minimal energy state. The most probable state treatment is on the other hand, a time independent estimate of the system configuration based upon constraints which are to be imposed on the system at some particular time. As will be seen, field-reversed equilibria are found to be most probable for certain values of the constraints imposed. These will generally be states of finite pressure tending to lower and lower pressure as the energy-to-helicity ratio is lowered. It will prove unnecessary to demand that the J_z profile be negative in order to obtain (most probable) reversed-field equilibria with small but finite pressure.

II. MOST PROBABLE STATES IN MAGNETOHYDRODYNAMICS

A. Most Probable Magnetohydrostatic Equilibria

As we have seen in Sec. B of Chapt. I, solution of the reduced equilibrium equation requires that two equilibrium functions be specified in order that the remaining quantities be determined. Out of this doubly infinite set of arbitrary profiles - leading to a doubly infinite number of magnetohydrodynamic equilibria - one then usually considers only those equilibria which give the smallest growth rates in a linear stability analysis.

Typically, the experimentalist does not have the exact profiles under his control, but he can control a few global parameters. Thus the relevant question becomes the following: suppose a few global parameters are known, what are the "most probable" equilibrium profiles consistent with the given information?

A procedure for determining MHD equilibria when only global information is avaiable, was recently proposed by Montgomery, Turner, and Vahala.[3] This method may be outlined as follows.

For the sake of simplicity it is assumed that the plasma is cylindrical and the equilibrium quantities depend only on the radius r.

The three fields $\underset{\sim}{B}$, $\underset{\sim}{A}$, and $\underset{\sim}{J}$ are all solenoidal. The six non-zero vector components (B_θ, B_z, J_θ, J_z A_θ, A_z) and the pressure are random functions or r but only certain pairs of these functions are independent. One seeks a most probable set of profiles subject to known values of energy (per unit length),

$$\mu_o E = \pi \int \underset{\sim}{B}^2 \, ds \tag{38}$$

magnetic helicity (also per unit length),

$$H = 2\pi \int \underset{\sim}{A} \cdot \underset{\sim}{B} \, ds \tag{39}$$

toroidal flux,

$$\Phi = \int B_z \, ds \tag{40}$$

and toroidal current

$$I = \int J_z \, ds \tag{41}$$

where the integrals are over the cross section of the cylinder. These constraints may be interpreted as experimental parameters or as constants of the motion. Energy and magnetic helicity are exactly conserved in ideal MHD. The toroidal flux must also be conserved when the plasma is contained in a conducting shell. The current I is often controllable by means of feedback circuitry or other experimental arrangements.

It will be convenient to express the variables in dimensionless form. One may define a characteristic field strength B_o and measure length in units of the cylinder radius. The dimensionless field and current are then defined as

$$\hat{B}_z = \frac{B_z}{B_o} \quad ; \quad \hat{J}_z = \frac{\mu_o a J_z}{B_o} \tag{42}$$

The dimensionless constraints are related by their physical counterparts by

$$\hat{\Phi} = \Phi/2\pi a^2 B_o \; ; \quad \hat{I} = \mu_o I/2\pi a B_o$$

$$\hat{E} = \frac{\mu_o E}{2\pi a^2 B_o} \; ; \quad \hat{H} = \frac{H}{2\pi a^3 B_o^2} \tag{43}$$

In dropping the caret notation from this point on, all relevant quantities will be assumed dimensionless unless otherwise noted.

It is most natural, from the form of the imposed constraints, to take as basic variables the independent fields J_z and B_z. The aim is then to construct the a priori probability associated with the realization of a particular macroscopic state characterized by the B_z and J_z profiles. To this end Montgomery, et al.[3] introduced a field-line model. The macroscopic state is described by a set of occupation numbers N_i^B, and N_i^J which count the number of field lines or current lines which pass through a small area Δ_i of the cylinder

cross section. To simplify the model as much as possible field and current lines of only one direction were allowed. This restricted all possible profiles of B_z, J_z to be non-negative functions.

The mean field values within a cell Δ_i are defined in terms of the occupation numbers by

$$J_{z_i} = \frac{\lambda N_i^J}{\Delta_i} \quad ; \quad B_{z_i} = \frac{\lambda N_i^B}{\Delta_i} \tag{44}$$

where λ is a small scaling parameter. The flux and current are given by

$$\Phi = \lambda N^B \quad ; \quad I = \lambda N^J \tag{45}$$

where $N^B = \Sigma N_i^B$ and $N^J = \Sigma N_i^J$ are the total numbers of lines.

Using standard Boltzmann combinatorics one can write an expression for the probability W_B that a particular set of occupation numbers N_i^B is realized for the B_z field, i.e.,

$$W_B = \text{const. x } N^B! \prod_i \frac{(\Delta_i)^{N_i^B}}{N_i^B!} \tag{46}$$

A similar expression results for the independent field J_z. Thus the joint probability for the (B_z, J_z) fields is

$$W = \text{const. x } N^B!N^J! \prod_i \frac{(\Delta_i)^{N_i^B + N_i^J}}{N_i^B!\, N_i^J!} \tag{47}$$

In this discrete representation the energy and helicity constraints are formulated in the following way. For the vector potential one is free to impose the condition $A_z(1) = 0$. (This is the natural boundary condition for the varational calculation which follows.) After integration by parts the energy and helicity take the form

$$E = \frac{1}{2} \int_0^1 r dr \left(B_2^{\,2} + A_z B_z \right) \tag{48}$$

$$H = 2 \int_0^1 r dr \, A_z B_z \tag{49}$$

One then solves for A_z in terms of J_z by constructing a symmetric Green's function $G(r,r')$ for which

$$\frac{1}{r} \frac{d}{dr} \left[r \frac{d}{dr} G(r,r') \right] = - \frac{1}{r} \delta(r - r') \tag{50}$$

with $G(r,r')$ regular at the origin and $G(1,r') = 0$. Thus

$$G(r,r') = \begin{cases} -\ln r' & (r < r') \\ -\ln r & (r > r') \end{cases} \tag{51}$$

In terms of J_z and $G(r,r')$,

$$A_z(r) = \int_0^1 r' dr' G(r,r') J_z(r') \tag{52}$$

For the discrete model the energy and helicity constraints are therefore written as

$$E = \lambda^2 \sum_i \frac{(N_i^B)^2}{\Delta_i} + \lambda^2 \sum_{ij} G_{ij} N_i^J N_j^J \tag{53}$$

$$H = \lambda^2 \sum_{ij} G_{ij} N_i^B N_j^J \tag{54}$$

where G_{ij} is the analog of $G(r,r')$ in this representation. Using Sterling's approximation to the factorials for large N, the log of the joint probability is approximately

$$\ln W \cong - \sum_i N_i^B \ln\left(\frac{N_i^B}{N^B \Delta_i}\right) - \sum_i N_i^J \ln\left(\frac{N_i^J}{N^J \Delta_i}\right) \tag{55}$$

We then seek the most probable state by maximizing lnW subject to given values of Φ, I, E, and H, and thereby obtain the variational conditions

$$\delta N_i^B \left[1 + \ln\left(\frac{N_i^B}{N^B \Delta_i}\right) + \alpha_B \lambda + 2\beta\lambda^2 \frac{N_i^B}{\Delta_i} + \frac{N_i^B}{N^B} + \gamma\lambda^2 \sum_j G_{ij} N_j^J \right] = 0 \tag{56}$$

$$\delta N_i^J \left[1 + \ln\left(\frac{N_i^J}{N^J \Delta_i}\right) + \alpha_J \lambda + 2\beta\lambda^2 \sum_j G_{ij} N_j^J + \frac{N_i^J}{N^J} + \gamma\lambda^2 \sum_j G_{ij} N_j^B \right] = 0 \tag{57}$$

where α_B, α_J, β, and γ are Lagrange multipliers associated with flux Φ, current I, energy E, and magnetic helicity H respectively. Making use of Eqs. (45) and (45) and setting the bracket ed expressions to zero, Eqs. (56) and (57) become

$$B_{zi} = \Phi \exp\left[\frac{-B_{zi}}{\Phi} \Delta_i - \lambda\left[1 + \alpha_B + 2\beta B_{zi} + \gamma \sum_j G_{ij} J_{zj} \Delta_j\right]\right] \tag{58}$$

$$J_{zi} = I \exp\left[- J_{zi}\Delta_i/I - \lambda \left[1 + \alpha_J + 2\beta \sum_j G_{ij} J_{zj} \Delta_j + \gamma \sum_j G_{ij} B_{zj} \Delta_j\right]\right] \tag{59}$$

Letting $\Delta_1 \to 0$ yields the continuum expressions

$$B_z(r) = \exp\left(-\alpha_B - \beta B_z(r) - \gamma A_z(r)\right) \tag{60}$$

$$J_z(r) = \exp\left(-\alpha_J - \beta A_z(r) - \gamma \Pi(r)\right) \tag{61}$$

where constants have been absorbed into the undetermined multipliers wherever possible. $\Pi(r)$ is an auxilliary variable whose definition, analogous to that of A_z, is

$$\Pi(r) = \int_0^1 r' dr' G(r,r') B_z(r') \tag{62}$$

Equations (60) and (61) together with the differential forms of the integral definitions of Π and A_z

$$\frac{d^2\Pi}{dr^2} + \frac{1}{r}\frac{d\Pi}{dr} = -B_z \tag{63}$$

$$\frac{d^2A_z}{dr^2} + \frac{1}{r}\frac{dA_z}{dr} = -J_z \tag{64}$$

and the boundary conditions

$$A_z(1) = \Pi(1) = 0 \tag{65}$$

(together with the requirement of regularity at the origin) determine the most probable B_z and J_z profiles. Having found these profiles, the remaining equilibrium quantities follow from Maxwell's equations, and the pressure is determined from the pressure balance equation which in this simple geometry is

$$\frac{dp}{dr} = -B_z\frac{dB_z}{dr} + B_\theta\frac{dB_\theta}{dr} - \frac{B_\theta^2}{r} \tag{66}$$

Equations (60) and (61) derived above are only appropriate if there is some reason to restrict the random functions B_z and J_z to the class of bounded non-negative functions. In many applications this assumption is not very severe. However, there are instances

in which such an assumption is too restrictive, e.g. the application to reversed-field pinch equilibria. The generalization of this method to include arbitrary functions with possibly negative behavior is not straight-forward. One possible generalization will be presented in Chapter III together with numerically computed solutions of the resulting differential equations. In the spirit of statistical methods, one should regard these "most probable" estimates for the equilibrium profiles as speculative. The merits of these models will ultimately depend upon how reasonable their predictions are when compared with experimental evidence. The purpose of this dissertation is not to make a detailed comparison with experiments, but to discover the basic features of solutions to the most probable equations in two main parameter regimes corresponding to the tokamak and the reversed-field pinch.

B. Analytical Solutions for Most Probable MHD Equilibria in the Case of Unconstrained Magnetic Helicity

In the most probable state equations (60)-(61) of Sec. A, any of the four constraints Φ, I, E, or H may be dropped by setting the associated Lagrange multiplier equal to zero. Consider the case in which both energy and helicity are unconstrained. Setting $\beta = \gamma = 0$, the result is

$$B_z = e^{-\alpha_B} = \text{constant} \tag{67}$$

$$J_z = e^{-\alpha_J} = \text{constant}. \tag{68}$$

Put simply, this means that if the only information available about the configuration where the flux Φ and the current I, the most reasonable guess about the state would be that the magnetic field and current density are uniform.

To obtain solutions in the case in which energy, flux, and current are constrained, but magnetic helicity is not, one sets $\gamma = 0$. Leaving γ arbitrary for the moment, we may take the derivative of Eq. (60) obtaining

$$\frac{dB_z}{dr} = \frac{-\gamma dA_z}{dr} \frac{\exp(-\alpha_B - \beta B_z - \gamma A_z)}{\left[1 + \beta \exp(-\alpha_B - \beta B_z - \gamma A_z)\right]} \tag{69}$$

Hence, for $\gamma = 0$, B_z is a constant determined by the flux Φ; i.e.

$$B_z = 2\Phi = \text{const.} \tag{70}$$

Using Eqs. (61) and (64) the system of equations thus reduces to the single equation for the vector potential

$$\frac{d^2A_z}{dr^2} + \frac{1}{r}\frac{dA_z}{dr} + \exp\left[-\alpha_J - \beta A_z\right] = 0 \tag{71}$$

subject to the boundary condition $A_z(1) = 0$. Montgomery, et al.[3] have shown that analytical solutions of this problem can be found.

Equation (71) is a one-dimensional version of a partial differential equation sometimes called Liouville's equation for which general solutions in one and two dimensions are known.[21] Letting $\theta = -\beta A_z$ and $-\beta \exp(-\alpha_J) \equiv \delta$, the equation takes a simpler form

$$\frac{d^2\theta}{dr^2} + \frac{1}{r}\frac{d\theta}{dr} + \delta e^{\theta} = 0 \qquad (72)$$

Its solution is

$$\theta = 2 \ln \left| (B + 1) / (Br^2 + 1) \right| \qquad (73) =$$

where $\delta = 8B/(B + 1)^2$ and B is a parameter which must be real and > -1.

The current and energy are readily calculated from the solution for θ by integrating

$$I = \int_0^1 r dr \, J_z = e^{-\alpha_J} \int_0^1 r dr e^{\theta} \qquad (74)$$

and

$$E = \frac{1}{2}\int_0^1 (B_z^2 + B_\theta^2)\, r dr$$

$$= 2\phi^2 + \frac{1}{2\beta^2}\int_0^1 r dr \left(\frac{d\theta}{dr}\right)^2 \tag{75}$$

For arbitrary ϕ one, for convenience, defines

$$B^2\xi_\perp \equiv \beta^2(2E - 4\phi^2) = \int_0^1 r dr \left(\frac{d\theta}{dr}\right)^2 \tag{76}$$

Upon integration

$$I = \frac{(1 + B)}{2} \exp(-\alpha_J) \tag{77}$$

$$\xi_\perp = \frac{8}{\beta^2}\left[\ln(1 + B) - B(B + 1)^{-1}\right] \tag{78}$$

with $\beta \exp(-\alpha_J) = -8B/(B + 1)^2$. Elimination of α_J and β gives a formula for the ratio

$$\frac{\xi_\perp}{I^2} = \frac{2(1 + B)^2}{B^2}\left[\ln(1 + B) - B(1 + B)^{-1}\right] \tag{79}$$

This ratio is a monotonic function of the parameter B. Thus, if one is

given I and ζ_1 the value of B is uniquely determined. In terms of this parameter the field profiles are explicitly

$$B_z(r) = 2\,\Phi = \text{const.} \tag{80}$$

$$B_\theta(r) = I\,\frac{(1+B)r}{(1+Br^2)} \tag{81}$$

$$J_z(r) = 2I(1+B)\,/\,(1+Br^2)^2 \tag{82}$$

$$p(r) = \frac{I^2}{2}\left[(2+B) - r^2\,(2+Br^2)\right]\,/\,(1+Br^2)^2 \tag{83}$$

Note that the pressure p(r) is determined from Eq. (83) together with the boundary condition p(1) = 0. The solution, so determined, is not mathematically constrained to be a non-negative function of r. Physically we will require $p(r) \geq 0$ for all r, and so will reject those most probable state profiles for B_z and J_z which lead to negative pressure. For the case of unconstrained magnetic helicity one sees from Eq. (83) that the pressure $p(r) \geq 0$ for all most probable states with constrained values of energy, current, and flux. It will be shown that there exist choices of the constraints E, I, Φ, H for which this will not be true (and hence these states will be rejected on physical grounds). Typical profiles for various values of B are reproduced from Ref. 3 in Fig. (1). Note that the pressure p(r) is always a monotonically decreasing function of r with a maximum on axis (r = 0).

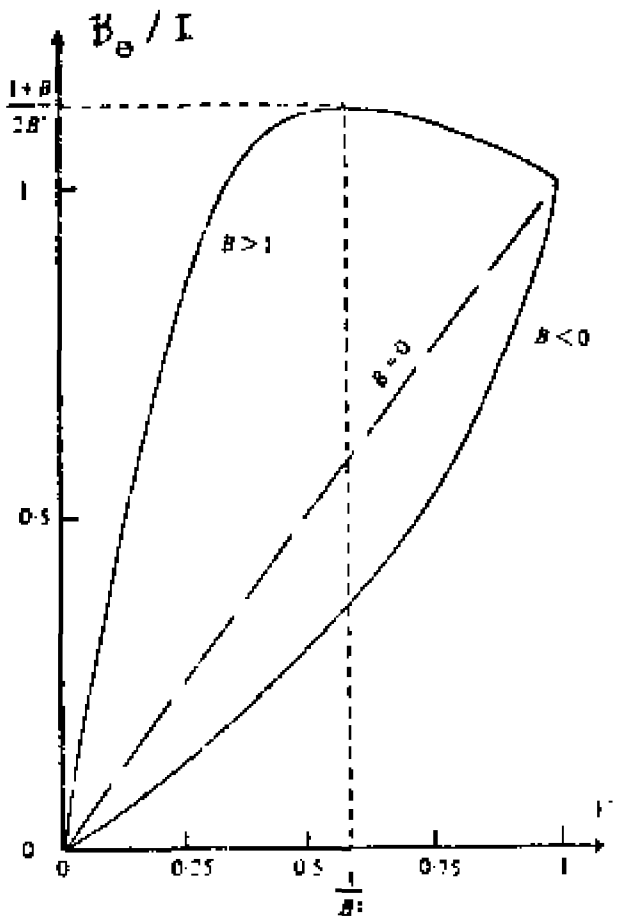

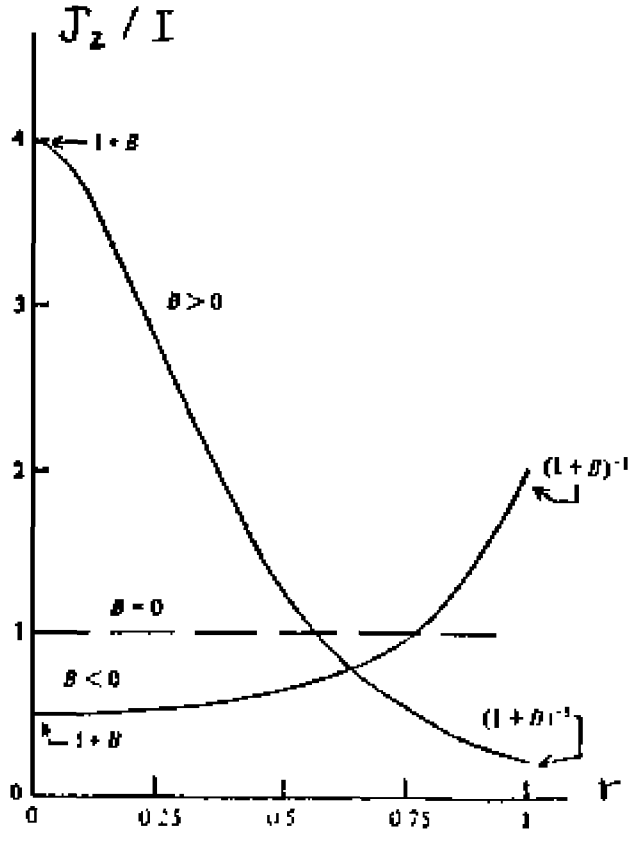

Fig. 1. Most Probable B_Θ and J_z profiles for unconstrained magnetic helicity ($\gamma \equiv 0$).

C. Force-Free States

It is of some interest to ascertain whether or not the Bessel function force-free states given by Eqs. (34)-(36) of Chapter I are obtainable, in some approximation, as solutions of the nonlinear, inhomogeneous most probable state equations (60)-(61); (63)-(65). Since the Bessel functions are solutions of a linear homogeneous differential equation, we shall examine linearized forms of Eqs. (60)-(61).

If for B_z and J_z, one assumes

$$B_z = B_o J_o(\lambda r) \tag{84}$$

$$J_z = \lambda B_z = \lambda B_o J_o(\lambda r) \tag{85}$$

then A_z and Π must satisfy

$$\Pi''(r) + \frac{1}{r}\Pi'(r) = -B_o J_o(\lambda r) \tag{86}$$

$$A_z''(r) + \frac{1}{r} A_z'(r) = -\lambda B_o J_o(\lambda r) \tag{87}$$

subject to the boundary conditions

$$A_z(1) = \Pi(1) = 0 \tag{88}$$

The solutions for Π and A_z are therefore

$$\Pi(r) = \frac{B_o}{\lambda^2}\left[J_o(\lambda r) - J_o(\lambda)\right] \tag{89}$$

$$A_z(r) = \frac{B_o}{\lambda}\left[J_o(\lambda r) - J_o(\lambda)\right] \tag{90}$$

By the definitions of the flux and current, the derivatives of Π and A_z at the boundary are

$$A_z'(1) = -I \quad ; \quad \Pi'(1) = -\Phi \tag{91}$$

Taking derivatives of Eqs. (89) and (90) one obtains

$$B_o J_1(\lambda) = \lambda\Phi = I \tag{92}$$

Thus the eigenvalue is determined by external conditions, i.e.

$$I / \Phi = \lambda \tag{93}$$

and the amplitude B_o is

$$B_o = I / J_1(\lambda) \tag{94}$$

One way of linearizing Eqs. (60) and (61) is to assume

$$\left| \alpha_B + \beta B_z + \gamma A_z \right| << 1 \tag{95}$$

$$\left| \alpha_J + \beta A_z + \gamma \Pi \right| << 1 \tag{96}$$

This allows one to write

$$B_z \overset{\sim}{=} 1 - \alpha_B - \beta B_z - \gamma A_z \tag{97}$$

$$J_z \overset{\sim}{=} 1 - \alpha_J - \beta A_z - \gamma \Pi \tag{98}$$

as approximations to Eqs. (60) and (61). Substituting Eqs. (84), (85), (89), and (90) into Eqs. (97) and (98) and equating the coefficients of $J_o(\lambda r)$ we obtain

$$1 + \beta + \gamma/\lambda = 0 \tag{99}$$

$$\lambda + \beta/\lambda + \gamma/\lambda^2 = 0 \tag{100}$$

while equating the constant terms gives

$$\alpha_B - \frac{\gamma B_o J_o(\lambda)}{\lambda} - 1 = 0 \tag{101}$$

$$\alpha_J - \left[\beta + \frac{\gamma}{\lambda}\right] \frac{B_o J_o(\lambda)}{\lambda} - 1 = 0 \tag{102}$$

Equations (99) and (100) can be satisfied simultaneously only if $\lambda = 1$. Thus from Eq. (93)

$$I = \Phi \tag{103}$$

Setting $\lambda = 1$ in either Eq. (99) or (100) one finds that β is arbitrary and that

$$\gamma = -(1+\beta) \tag{104}$$

The remaining Lagrange multipliers are determined from Eqs. (101) and (102):

$$\alpha_B = 1 - (\beta + 1) I \frac{J_o(1)}{J_1(1)} \tag{105}$$

$$\alpha_J = 1 - I \frac{J_o(1)}{J_1(1)} \tag{106}$$

Thus the assumptions (95) and (96) allow force-free solutions of the form

$$B_z = I \frac{J_o(r)}{J_1(1)} = J_z(r) \tag{107}$$

$$B_\theta = \frac{I}{J_1(1)} J_1(r) \tag{108}$$

Equations (97) and (98) are not the only linearized forms possible, however. If one makes a different assumption:

$$| \beta B_z + \gamma A_z | << 1 \tag{109}$$

$$| \beta A_z + \gamma \Pi | << 1 \tag{110}$$

then

$$B_z \cong k^2 (1 - \beta B_z - \gamma A_z) \tag{111}$$

$$J_z \cong \ell^2 (1 - \beta A_z - \gamma \Pi) \tag{112}$$

where

$$k^2 \equiv e^{-\alpha_B} \tag{113}$$

$$\ell^2 \equiv e^{-\alpha_J} \tag{114}$$

Substituting Eqs. (84), (85), (89), and (90) into the linear forms (111) and (112) and equating the coefficients of $J_o(\lambda r)$,

$$1 + k^2 (\beta + \gamma/\lambda) = 0 \tag{115}$$

$$\lambda + \frac{\ell^2}{\lambda} (\beta + \gamma/\lambda) = 0 \tag{116}$$

while equating the constant terms yields

$$k^2 \left(1 + \frac{\gamma}{\lambda} B_o J_o(\lambda)\right) = 0 \tag{117}$$

$$\ell^2 \left| 1 + (\beta + \frac{\gamma}{\lambda}) \frac{B_o J_o(\lambda)}{\lambda} \right| = 0 \tag{118}$$

where λ is given by Eq. (93) and B_o by Eq. (94). From Eq. (115)

$$(\beta + \gamma/\lambda) = -1/k^2 \tag{119}$$

which according to Eq. (116) implies

$$\ell^2 = \lambda^2 k^2 \tag{120}$$

Solving for γ in Eq. (117) (with $k^2 \neq 0$) gives

$$\gamma = -\lambda \; / \; B_o J_o(\lambda) \tag{121}$$

and substituting for γ into Eq. (118) ($\ell^2 \neq 0$) one obtains

$$\beta = (1 - \lambda) \; / \; B_o J_o(\lambda) \tag{122}$$

The value of k^2 from Eqs. (119), (120), (121), and (122) is

$$k^2 = B_o J_o(\lambda) \; / \; \lambda \tag{123}$$

and therefore

$$\ell^2 = \lambda B_o J_o(\lambda) \tag{124}$$

Values of the Lagrange multipliers α_B and α_J then follow from the definitions (113)-(114). Thus the assumptions (109) and (110) allow force-free state solutions of the form

$$B_z = \frac{I}{J_1(\lambda)} \; J_o(\lambda r) \tag{125}$$

$$B_\theta = \frac{I}{J_1(\lambda)} \; J_1(\lambda r) \tag{126}$$

for arbitrary $\lambda < 2.4$. This upper bound on λ is required since, by

assumption $B_z(r) \geq 0$, and $J_z(r) \geq 0$ for all r. Note that the values of β and λ given by Eqs. (121) and (122) are singular at $\lambda = 2.4$.

To check that the linearity conditions are met, we write for linearizations of the first type

$$B_z \simeq 1 + \eta_1 \tag{127}$$

$$J_z \simeq 1 + \xi_1 \tag{128}$$

where

$$\eta_1 = -\alpha_B - \beta B_z - \gamma A_z \tag{129}$$

$$\xi_1 = -\alpha_J - \beta A_z - \gamma \Pi \tag{130}$$

Integrating (127) and (128) gives

$$\Phi \simeq \frac{1}{2} + \int_0^1 r dr \ \eta_1 \equiv \frac{1}{2} + \langle \eta_1 \rangle \tag{131}$$

$$I \simeq \frac{1}{2} + \int_0^1 r dr \ \xi_1 \equiv \frac{1}{2} + \langle \xi_1 \rangle \tag{132}$$

and solving for the averages

$$\langle \eta_1 \rangle \overset{\sim}{=} \Phi - \frac{1}{2} \tag{133}$$

$$\langle \xi_1 \rangle \overset{\sim}{=} I - \frac{1}{2} \tag{134}$$

(where $I = \Phi$ in this case).

For linearizations of the second type, we let

$$B_z \overset{\sim}{=} k^2 (1 + \eta_2) \tag{135}$$

$$J_z \overset{\sim}{=} \ell^2 (1 + \xi_2) \tag{136}$$

where

$$\eta_2 \equiv -\beta B_z - \gamma A_z \quad ; \quad \xi_2 \equiv -\beta A_z - \gamma \Pi \tag{137}$$

Integrations yields

$$\Phi/k^2 = \frac{1}{2} + \int_0^1 r dr\, \eta_2 \equiv \frac{1}{2} + \langle \eta_2 \rangle \tag{138}$$

$$I/\lambda^2 k^2 = \frac{1}{2} + \int_0^1 r dr\, \xi_2 = \frac{1}{2} + \langle \xi_2 \rangle \tag{139}$$

and solving for $\langle \eta_2 \rangle$ and $\langle \xi_2 \rangle$

$$\langle \eta 2 \rangle \cong \phi/k^2 - \frac{1}{2} \tag{140}$$

$$\langle \xi_2 \rangle \cong I/\lambda^2 k^2 - \frac{1}{2} \tag{141}$$

Substituting for k^2 and ϕ from Eqs. (93) and (123) shows that the averages depend only on λ, i.e.

$$\langle \eta_2 \rangle \cong \frac{J_1(\lambda)}{J_o(\lambda)} - \frac{1}{2} \tag{142}$$

$$\langle \xi_2 \rangle \cong \frac{J_1(\lambda)}{\lambda J_o(\lambda)} - \frac{1}{2} \tag{143}$$

The relative error ε made in approximating exp (δ) by $(1 + \delta)$ for some small number $\delta > 0$ can be found by computing

$$\varepsilon = \frac{e^{\delta} - (1 + \delta)}{e^{\delta}} \tag{144}$$

A table of ε for various $\delta < 1$ is shown below.

Table 1

δ	ε in percent
0.0	0.0
0.1	0.4
0.2	1.8
0.3	3.7
0.4	6.2
0.5	9.0

If one identifies $|\langle\eta\rangle|$ and $|\langle\xi\rangle|$ with δ, then the error made in approximating the exponentials in Eqs. (60) and (61) by linear forms can be estimated from table 1. Demanding an error of less than 10% restricts the magnitudes of the averages $|\langle\eta\rangle|$ and $|\langle\xi\rangle|$ to be not much more than 0.5. For linearizations of the first type Eqs. (133) and (134) suggest that for a 10% error the values of I or Φ be less than one. For linearized forms of the second type we refer to table 2 below, in which the values of $\langle\eta_1\rangle$ and $\langle\xi_1\rangle$ are shown for $0.1 \leq \lambda \leq 2.1$.

Table 2

λ	$\langle\eta_2\rangle$	$\langle\xi_2\rangle$
0.1	-0.45	0.00025
0.3	-0.35	0.004
0.5	-0.24	0.02
0.7	-0.13	0.03
0.9	0.003	0.06
1.1	0.16	0.10
1.3	0.34	0.15
1.5	0.59	0.23
1.7	0.95	0.35
1.9	1.56	0.59
2.1	2.91	1.12

These values indicate that a 10% error tolerance would restrict λ to be less than 1.4. In Sec. F of this chapter, examples of approximate force-free solutions of the most probable state equations will be presented and compared with the predictions of this section.

D. Numerical Method

Equations (60)-(61); (63)-(65), together with conditions of regularity at the origin represent a two point boundary value problem for a fourth order system of coupled, nonlinear, ordinary differential equations. The usual method of solution is to integrate the equations using a single step method (such as the Runge-Kutta algorithm). Regularity at the origin may be guaranteed by expanding A_z and Π to leading order in r, i.e., near $r = 0$

$$A_z = a_o + a_2 r^2 \quad ; \qquad \Pi = p_o + p_2 r^2 \tag{145}$$

The coefficients a_2 and p_2 are found by substitution giving

$$p_2 = -\frac{1}{4} b_o \tag{146}$$

$$a_2 = -\frac{1}{4} \exp\left(-\alpha_J - \beta a_o - \gamma p_o\right) \tag{147}$$

where $b_o \equiv B_z(0)$ and

$$b_o = \exp(-\alpha_\beta - \beta b_o - \gamma a_o) \tag{148}$$

The initial values a_o and p_o may then be adjusted to satisfy the boundary conditions at r = 1 after a number of inerations. A modification of Brown's method[22] was used for this purpose. Brown's method is a quadratically convergent algorithum similar to Newton's, but requiring fewer function evaluations per iterative step. The modified algorithum is derivative-free. The specific program ZSYSTEM was obtained from the IMSL program library.[23]

From the definitions of Φ, and I one finds upon integration that

$$\frac{dA_z(1)}{dr} = - I \tag{149}$$

$$\frac{d\Pi}{dr}(1) = - \Phi \tag{150}$$

Therefore, if one specifies Φ and I at the beginning of the computation, boundary conditions on the derivatives of Π and A_z are automatically prescribed. One may use the two parameters, α_β, and α_J to satisfy these additional conditions leaving β and γ as the only free parameters. The analytic solution of Sec. B for $\gamma = 0$ (unconstrained magnetic helicity) are useful as a starting point, and also as a check on the accuracy of computation. From such a solution γ

may be incremented in small steps to obtain other solutions. The output of the numerical algorithm must satisfy two criteria to be considered a solution. First, the error made in approximating the continuous integrals of the equations by a discrete numerical method must be within acceptable limits. Secondly, the boundary conditions must be met to within an acceptable error tolerance. The solution of Eqs. (63) - (65) to be presented, were integrated using a variable step differential equation solver DASCRU, obtained from the IMSL library. DASCRU has automatic error estimating capabilities which guarantee a global relative error of less than 10^{-4}. The program ZSYSTEM was then allowed to iterate on integrals obtained by DASCRU until the boundary conditions were met to within an absolute error of 10^{-5}.

Unfortunately it is difficult to specify the energy and helicity in addition to the flux and current in order to obtain numerical solutions. The reason is that each Lagrange multiplier, eliminated in favor of its corresponding constant by Brown's algorithm, adds another dimension to the space to be scanned by ZSYSTEM and thereby increases the possibility that the alogrithm will wander from the solution sought and fail to converge. This is a well known problem associated with Newton's method even in one dimension. The strategy adopted here is to obtain solutions with fixed flux Φ and current I for various values of the Lagrange multipliers β and γ after which the values of energy E and magnetic helicity H may be

found by numerically integrating these solutions. One thus hopes to ascertain the influence of these constraints on the solutions by mapping β and γ onto the constants E and H. Because of the large number of imposed constraints it is hoped that this mapping is one-to-one, although a theoretical proof is lacking.

In the surveys of solutions to be presented, the values of the parameter β are chosen by reference to the parameter B which determines the solutions for unconstrained helicity (Eqs.(80)-(83). For $\gamma = 0$ the relation is

$$\beta = \frac{-4B}{(B + 1)\ I} \tag{151}$$

showing that β scales inversely with I for a given B. It is also obvious from this relation that when $B \gtrsim 10$, β is more or less independent of B, assymptotically approaching $\beta = -4/I$. Some preliminary computations showed that no significant qualitative change occurred in solutions for a fixed β when $|\gamma|$ was greater than two or three times $|\beta|$. Therefore our adopted numerical procedure for the subsequent surveys is the following: Using the analytic solutions for $\gamma = 0$ as a start, we choose β for a given I within a range corresponding to $-1 < B \leq 10$. We then move outward from $\gamma = 0$ until $|\gamma| \sim 3|\beta|$. This, it is expected, will give a good indication of the behavior of solutions for all β and γ.

E. Numerical Results for Unit Flux and Current, (ϕ I = 1)

To reveal basic trends of the solutions to the most probable state equations, we first examine the case in which $\Phi = I = 1$. In terms of the physically measured flux and current, (denoted by asterisks) this choice implies the special relationship

$$\mu_o a\, I^* = \phi^* \tag{152}$$

The characteristic magnetic field is left unspecified, and any particular choice defines ϕ^* according to

$$\phi^* = 2\pi a^2 B_o \tag{153}$$

If one takes $B_o \sim B_T(a)$ then the safety factor is

$$q(a) \sim \frac{a}{R} \tag{154}$$

These parameters may thus represent a tokamak ($q > 1$) with a current that is greater than normal by a factor of $(R/a)^2$. To interpret another way, since $\Theta = I/2\Phi = 1/2$, one may think of these values as representative of a stabilized Z-pinch ($\Theta \sim 1$) with half the usual current.

The qualitative behavior of the solutions, depicted in Fig. (2-4), seem to depend in large measure upon the quadrant of the β-γ

plane from which these two Lagrange multipliers are chosen. Beginning with $\beta < 0$, and $\gamma > 0$ in Fig. (2(a)) one finds a paramagnetic profile for B_z and a current strongly peaked on the axis. (In common usage, the word paramagnetic describes a plasma which enhances the magnetic field as indicated by a B_z profile which decreases with radius. The opposite situation is termed diamagnetic.) Keeping β fixed while decreasing γ causes the B_z profile to flatten to a uniform field at $\gamma = 0$ and then to become diamagnetic as in Fig. (2(b)) for $\gamma < 0$. The behavior of the J_z profile is generally unaffected. At the opposite quadrant where $\beta > 0$, and $\gamma > 0$ solutions resemble the one shown in Fig. (3(a)). Here B_z is diamagnetic as for $\beta > 0$, $\gamma > 0$ but J_z is peaked at the boundary as it would be for a sheet-like current. Decreasing γ for $\beta > 0$ again flattens the B_z profile to a constant field at $\gamma = 0$ and then switches to paramagnetic B_z for $\gamma < 0$ (Fig. 3(b)). During this transition J_z also flattens and changes to a profile peaked on axis. Penetration of the current to the center of the plasma occurs when $\gamma < 0$. A glance at Figs. (4(a)) - (4(b)) reveals that the solutions for unconstrained energy ($\beta = 0$) belong to the same category as those for $\beta > 0$. The transition in B_z for a fixed γ occurs at small negative values of β.

The global constants E and H are functions of β and γ. Their dependence on the parameters is shown in Fig. (5(a)) and (5(b)) plotted against γ for different values of β. The limited domain of some of the curves is of significance. The endpoints represent the

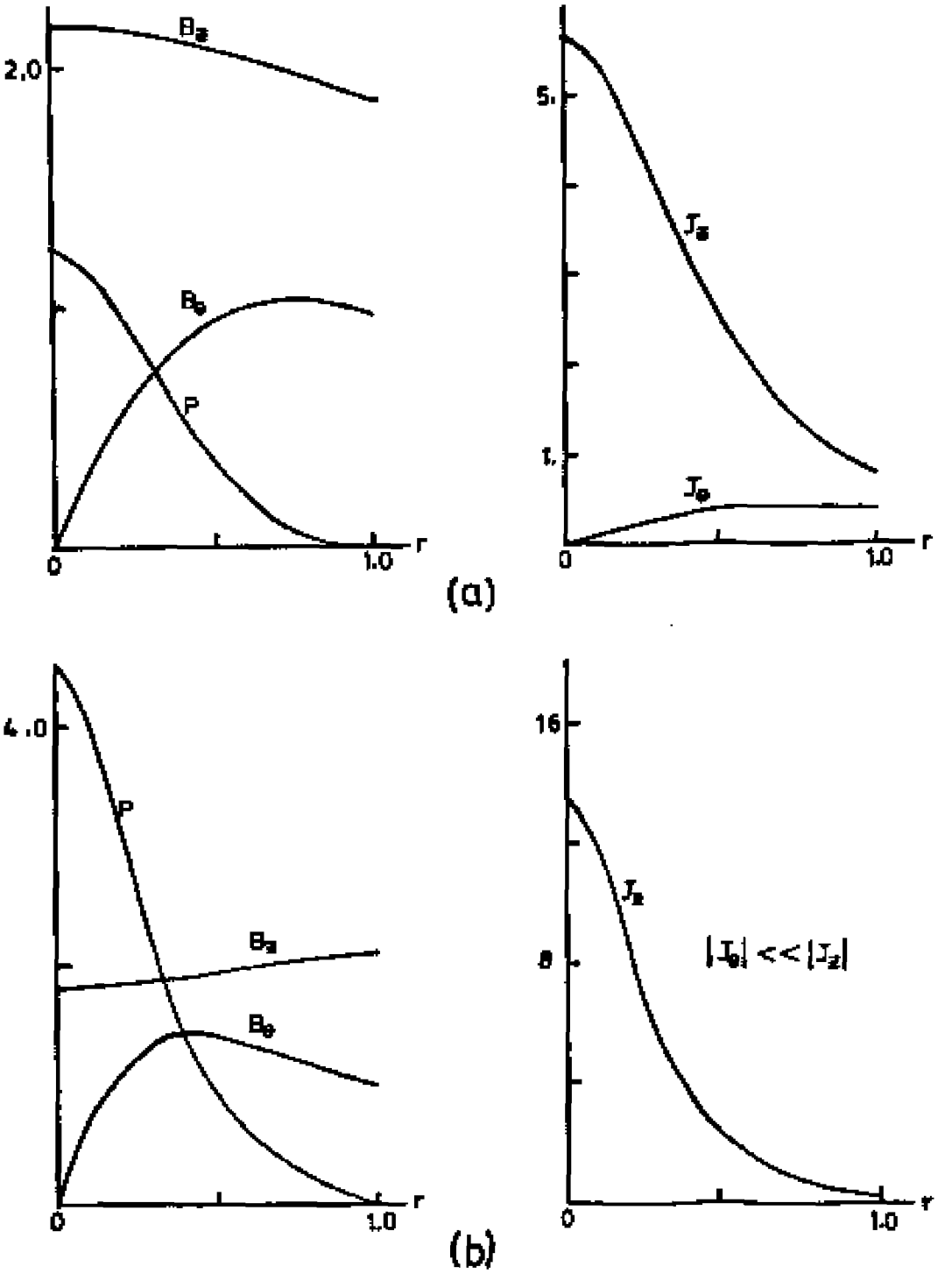

Fig. 2. Typical most probable equilibria for $\phi = I = 1$ when (a) $\beta < 0$, $\gamma > 0$; and (b) when $\beta < 0$, and $\gamma < 0$.

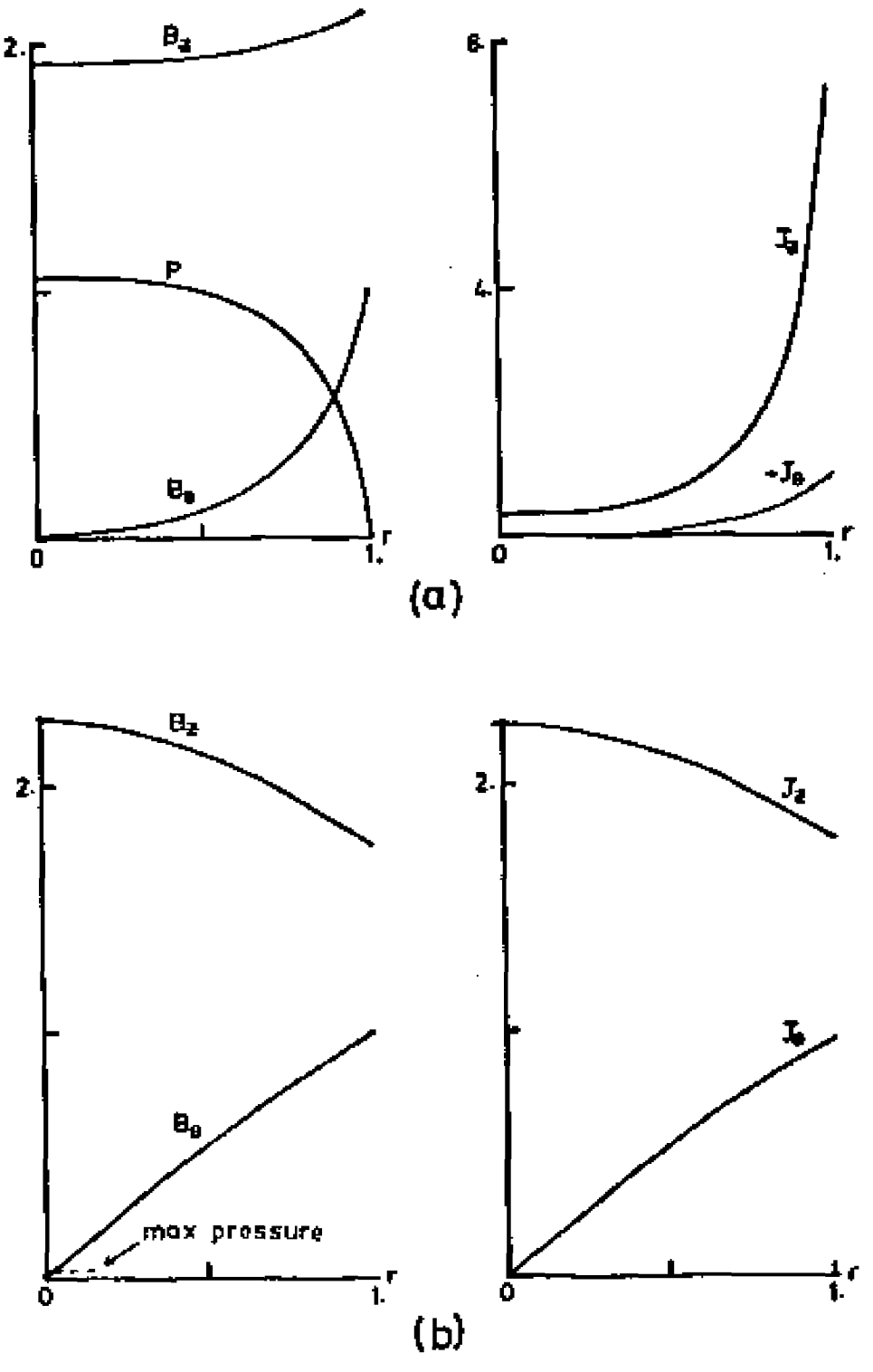

Fig. 3. Typical most probable equilibria for $\Phi = I = 1$ (a) when $\beta > 0$, and $\gamma > 0$; (b) when $\beta > 0$ and $\gamma < 0$.

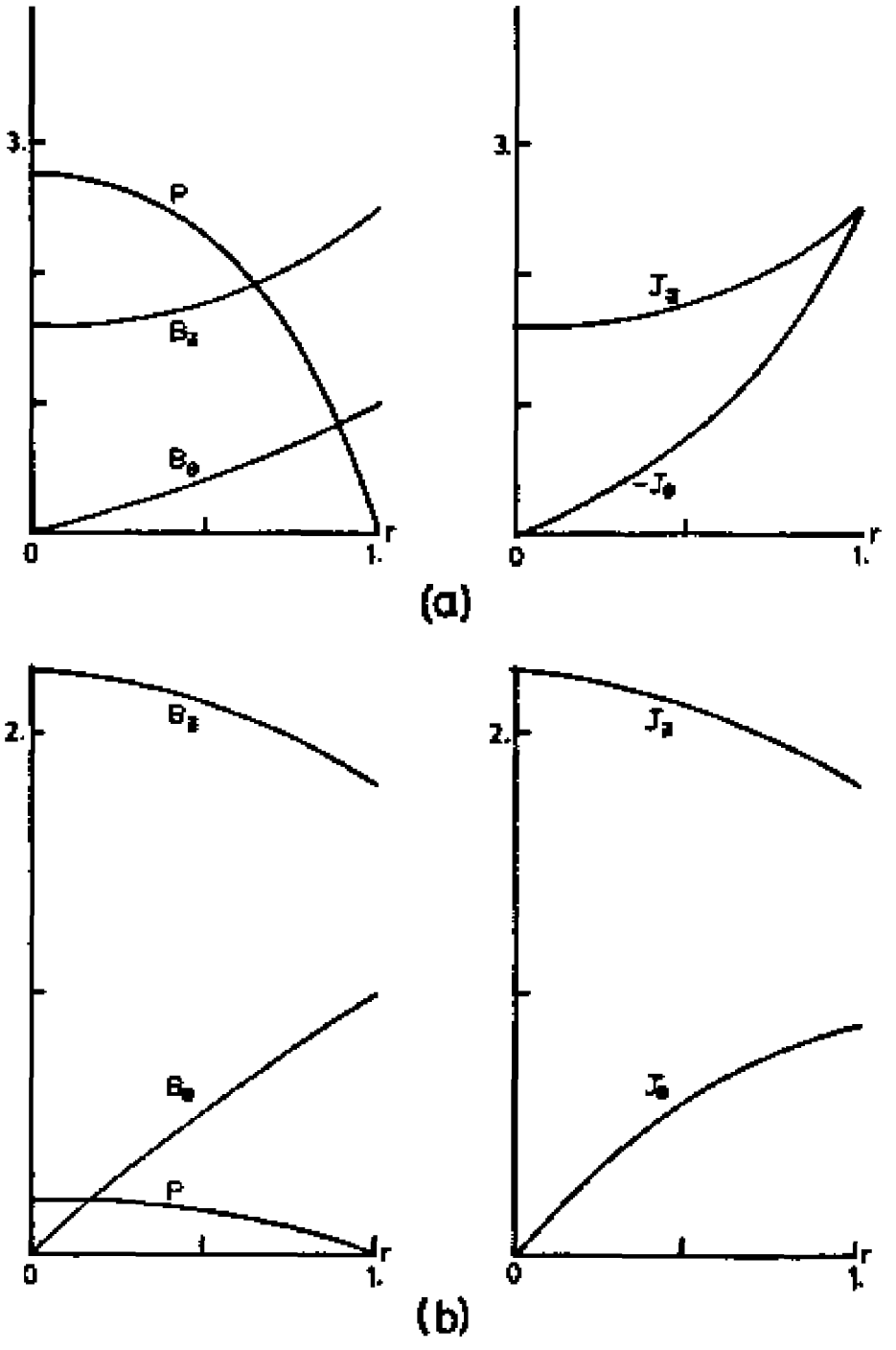

Fig. 4. Typical most probable equilibria for $\Phi = I = 1$ (a) when $\beta = 0$, and $\gamma > 0$; (b) when $\beta = 0$, and $\gamma < 0$.

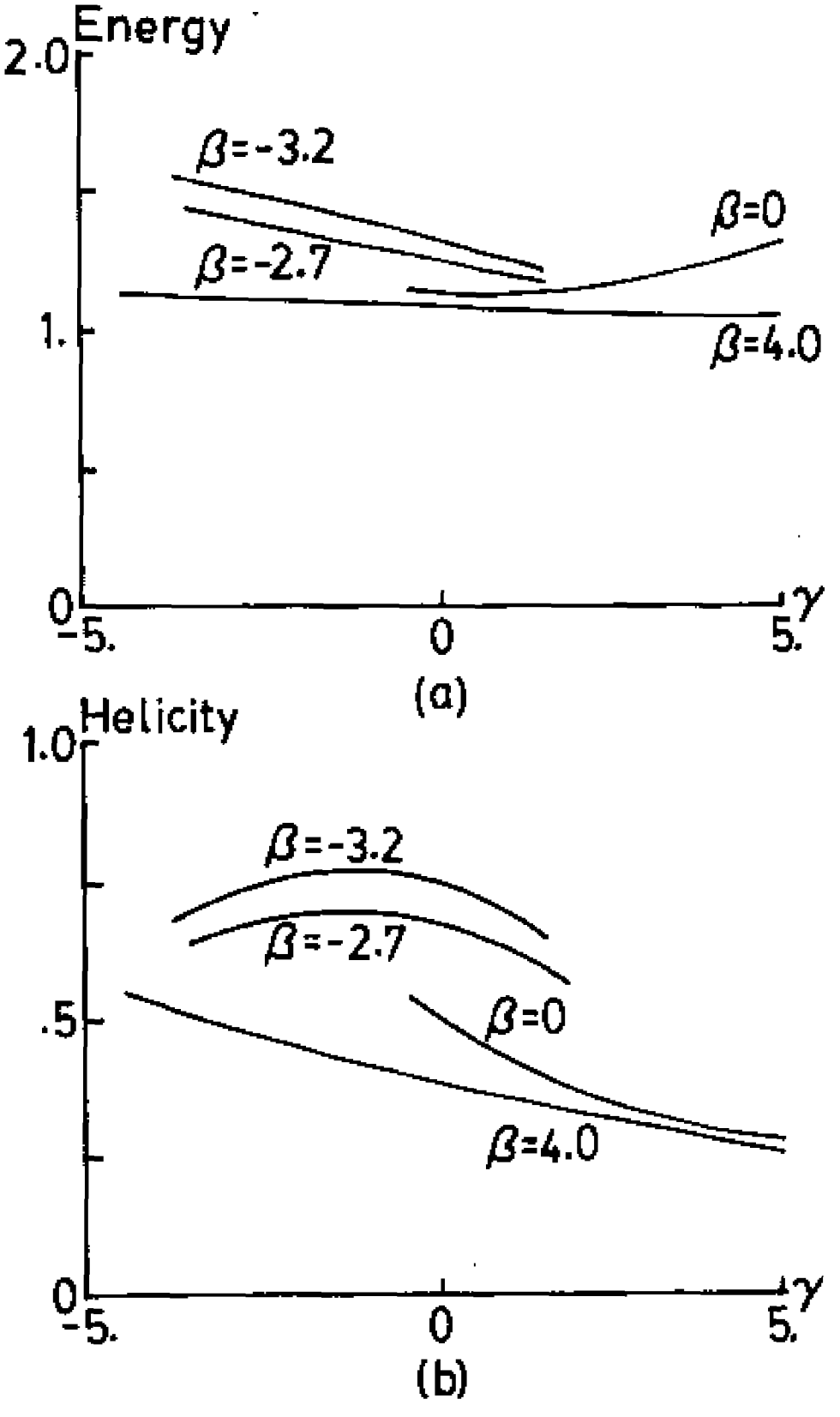

Fig. 5. Dependence of (a) energy and (b) magnetic helicity on the Lagrange multiplier γ for various values of β.

value of γ at which the equilibrium pressure profiles become negative. Negative pressures occur in this model, as discussed earlier, because the most probable B_z and J_z profiles are selected from the class of positive definite functions, and the equilibrium pressure profiles are calculated a posteriori from the requirements of the pressure balance equation (Eq.(66)). Thus there is no guarantee that a physically acceptable equilibrium exists for all values of the global constraints.

One further piece of information included in this survey is a plot of the energy to helicity ratio as a function of γ for various β shown in Fig. (6). For values of $\beta > 0$ a minimum usually occurs at the left endpoint of the curves, while for $\beta < 0$ the minimum values of E/H is found in the interior.

F. Quasi-Force-Free-Solutions

In this section we shall investigate the predictions of Sec. C regarding the existence of force-free solutions to the nonlinear most probable state equations. Once the flux and current have been selected, the procedure for obtaining quasi-force-free solutions numerically is to increment the Lagrange multiplier γ (at fixed β) in the direction of the analytically predicted value of γ, starting from $\gamma = 0$. The usual tendency of solutions, in these runs, is to exhibit smaller and smaller pressures until (unphysical) negative pressures are obtained.

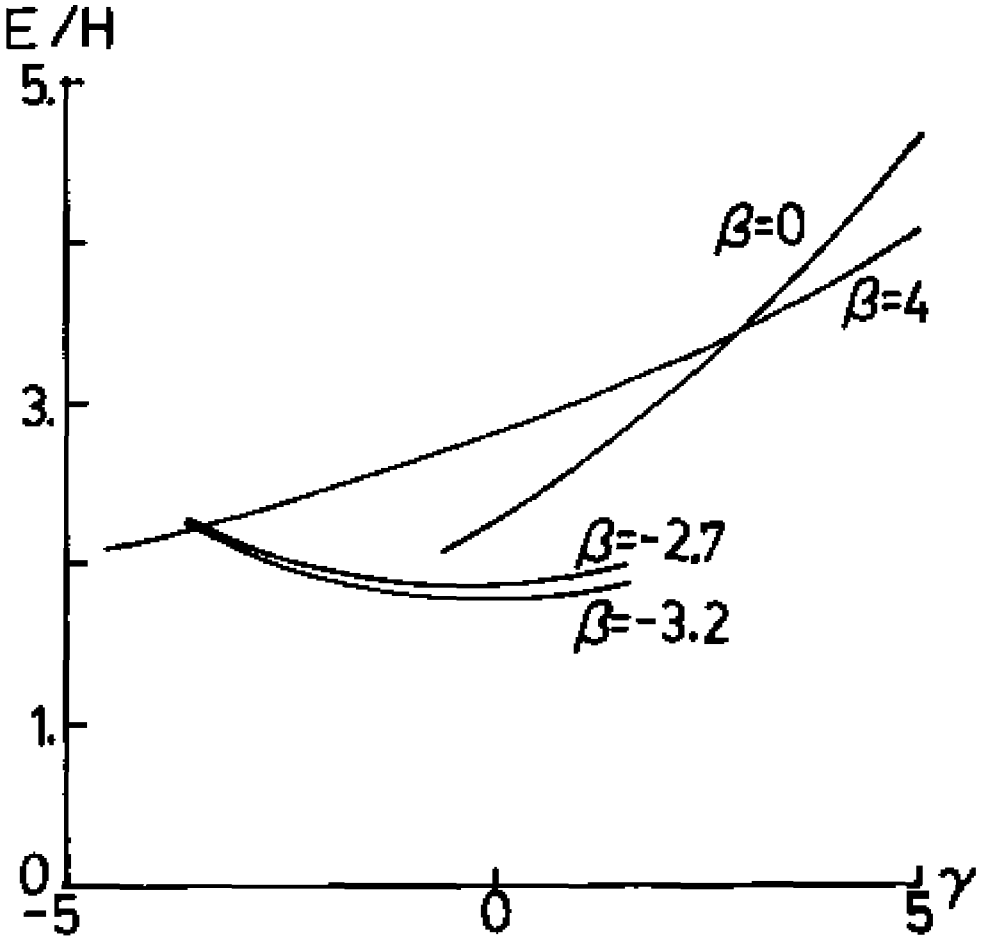

Fig. 6. Dependence of the energy to helicity ratio on the Lagrange multiplier γ for various β.

The quasi-force-free solution is then taken to be that with the smallest maximum pressure such that $p(r) \geq 0$ for all r.

In Sec. C it was shown that linearized forms of one type (Eqs. (97) and (98)) allow force-free solutions with $I = \Phi$ and $\lambda = 1$. These solutions are expected for any value of β. We present three solutions of this type found numerically from the full nonlinear system Eqs. (60)-(61); (63)-(65). One of these solutions is shown below in Table 3, with the values of the fields at selected points compared with the Bessel function solutions. Other data in Table 4 include the analytic values of the Lagrange multipliers (subscript zero) versus their values for the computed solutions (subscript c); the maximum plasma beta, β_{pl}; and the largest values of η_1 and ξ_1, where

$$\eta_1 = -\alpha_B - \beta B_z - \gamma A_z \tag{155}$$

$$\xi_1 = -\alpha_J - \beta A_z - \gamma \Pi \tag{156}$$

A graphic comparison is provided by Fig. (7) in which the local relative deviation $\varepsilon(r)$ of the numerical solutions from the Bessel function solutions, is plotted as a function of r, where $\varepsilon(r)$ is given by

Table 3

r	$B_z(r)$	$B_\theta(r)$	$J_z(r)$	$J_\theta(r)$	$B_0J_0(r)$	$B_0J_1(r)$
0.0	1.135	0.0	1.132	0.0	1.136	0.0
0.2	1.123	0.1126	1.120	0.1127	1.125	0.1131
0.4	1.090	0.2217	1.085	0.2212	1.091	0.2227
0.6	1.035	0.3241	1.031	0.3218	1.036	0.3258
0.8	0.9620	0.4174	0.9624	0.4110	0.9616	0.4191
1.0	0.8720	0.5000	0.8846	0.4865	0.8694	0.5000

Table 4

	β	γ_0	γ_c	α_{B_0}	α_{B_c}	α_{J_0}	α_{J_c}	max $\lvert\eta_1\rvert$	max $\lvert\xi_1\rvert$	max β_{pl}
$\phi = I = \frac{1}{2}$	-4.0	3.0	2.9	3.61	3.62	0.131	0.151	0.138	0.155	.0145
	8.0	-9.0	-8.9	-6.82	-6.84	0.131	0.123	0.137	0.124	.0051
$\phi = I = 1$	4.0	-5.0	-4.4	-7.69	-7.55	-0.737	-0.582	0.818	0.808	.009

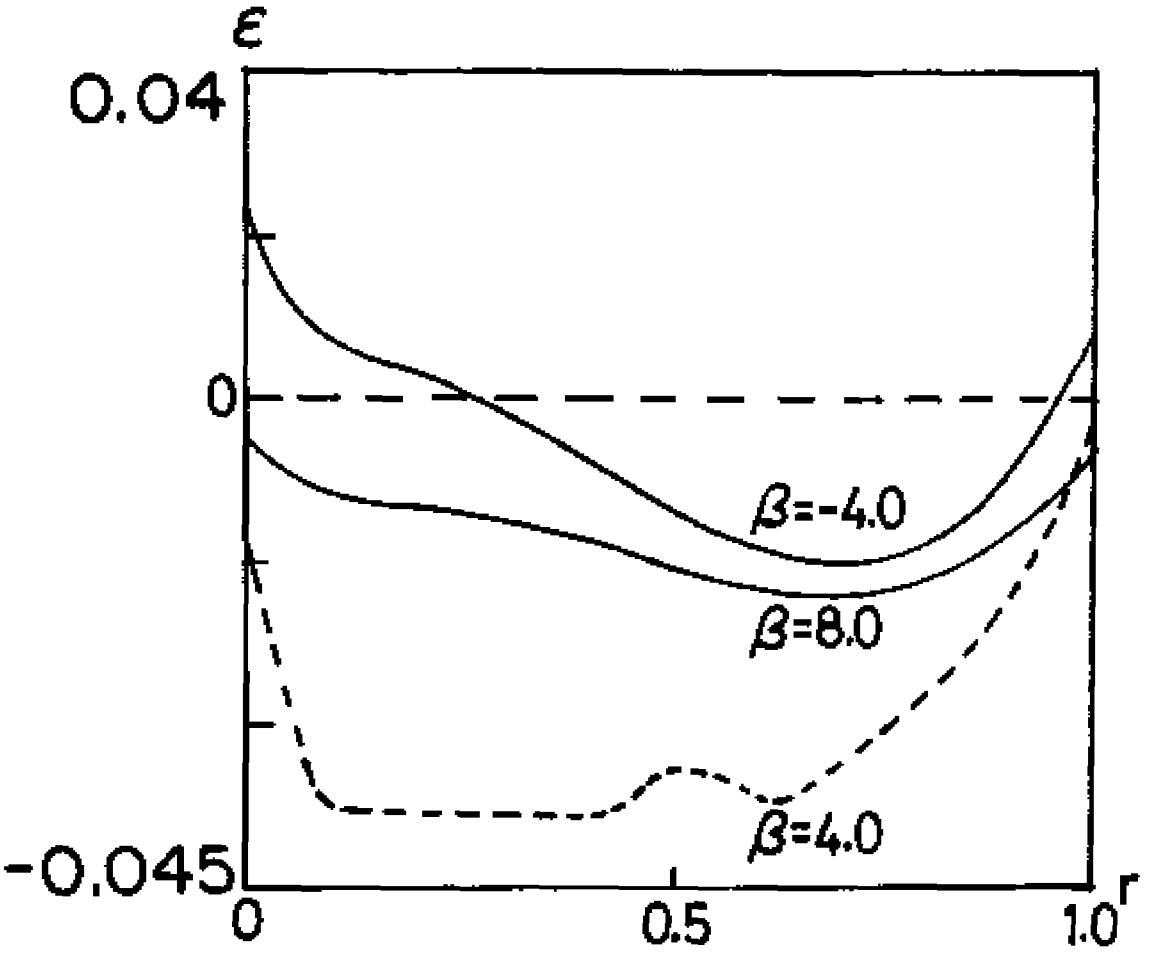

Fig. 7. The local relative deviation $\varepsilon(r)$ of the numerically computed solutions from Bessell function force-free states for linearized most probable state equations of the first type (Eqs. (97) and (98)). The solid curves are solutions for $\phi = I = 1/2$. The broken curve represents a $\phi = I = 1$ solution.

$$\epsilon(r) = \frac{(B_z(r) - B_o J_o(\lambda r)}{B_o J_o(\lambda r)} + \frac{(J_z(r) - \lambda B_o J_o(\lambda r))}{\lambda B_o J_o(\lambda r)}$$

$$+ \frac{(B_\theta(r) - B_o J_1(\lambda r))}{B_o J_1(\lambda r)} + \frac{(J_\theta(r) - \lambda B_o J_1(\lambda r))}{\lambda B_o J_1(\lambda r)} \qquad (157)$$

Comparing first the two solutions at $\Phi = I = \frac{1}{2}$, one finds that, although β is arbitrary according to the linear analysis of Sec. C, the numerical solution for $\beta > 0$ is more nearly force-free than the solution for $\beta < 0$. This can be seen by comparing the maximum plasma beta β_{pl} for each solution in Table 4. One also notices that the computed (nonlinear) values of the Lagrange multipliers are nearer the analytic (linear) values for $\beta > 0$ than for $\beta < 0$. These results are typical. Higher order nonlinear effects are presumed to be responsible for the dependence of the computed solutions on the Lagrange multiplier β. According to Sec. C, the linearity assumption should not be as well satisfied for $I = \Phi = 1$ as for $I = \Phi = \frac{1}{2}$. Referring to Table 4 one notices that the maximum values of η_1 and ξ_1 are only slightly less than one for $I = \Phi = 1$. The effects upon the solution are a higher value of β_{pl}, and poor agreement between the computed values of the Lagrange multipliers and their anticipated values from the linear analysis. From Fig. (7) one sees that this solution ($I = \Phi = 1$) has a greater deviation from the analytic force-free state than either of the solutions for $I = \Phi = \frac{1}{2}$.

Computed solutions corresponding to linearizations of the second form (Eqs. (111) and (112) have also been compared, at various λ, to the linear force-free-states. For this comparison Φ is held fixed at $\Phi = 1$ and I is varied to obtain solutions with different λ. Table 5 shows an example for $\lambda = 0.5$, and Table 6 lists relevant data for four solutions with λ ranging from 0.5 to 2.0. As λ increases beyond $\lambda = 1.0$, the discrepancies between the computed values of the Lagrange multipliers and the anticipated values become larger; the plasma beta, β_{pl} increases; and the maximum values of η_2 and ξ_2 (which must be small compared to one to permit linearization) increase and eventually become greater than one. These tendencies confirm the estimates of Sec. C that solutions of the nonlinear equations should become less nearly force-free as λ increases above 1.0. Figure (8) is a graphic comparison of these solutions with respect to the local relative deviation $\epsilon(r)$. Note the increasing amplitude of the deviations as λ increases.

On the basis of the foregoing results, the predictions of the linear analysis of Sec. C seem largely valid. Linearizations of the first type in which $I = \Phi$ and $\lambda = 1$ are nearly force free when $\Phi \leq 1$. Quasi-force-free states corresponding to linearizations of the second form seem limited to values of $\lambda \leq 1.2$.

Table 5

r	$B_z(r)$	$J_z(r)$	$B_\theta(r)$	$B_0J_0(\lambda r)$	$\lambda B_0J_0(\lambda r)$	$B_0J_1(\lambda r)$
0.0	2.065	1.065	0.0	2.064	1.032	0.0
0.2	2.060	1.058	0.1061	2.059	1.030	0.1031
0.4	2.044	1.043	0.2106	2.043	1.022	0.2053
0.6	2.017	1.017	0.3120	2.018	1.009	0.3061
0.8	1.982	0.9820	0.4089	1.982	0.9910	0.4046
1.0	1.937	0.9392	0.5000	1.937	0.9685	0.5000

Table 6

λ	$\beta_0=\beta_c$	γ_0	γ_c	α_{B_0}	α_{B_c}	α_{J_0}	α_{J_c}	max $\lvert\eta_2\rvert$	max $\lvert\xi_2\rvert$	max β_{pl}
0.5	0.258	-0.258	-0.375	-1.354	-1.161	0.031	0.062	0.500	0.123	0.0017
1.0	0.0	-0.575	-0.495	-0.553	-0.561	-0.553	-0.561	0.264	0.264	0.0150
1.2	-0.124	-0.742	-0.438	-0.298	-0.301	-0.663	-0.716	0.584	0.320	0.0440
2.0	-1.288	-2.576	1.000	0.946	1.327	-0.440	-0.869	2.371	1.056	0.4921

$$|\eta_2| \equiv |-\beta B_z - \gamma A_z|$$

$$|\xi_2| \equiv |-\beta A_z - \gamma \pi|$$

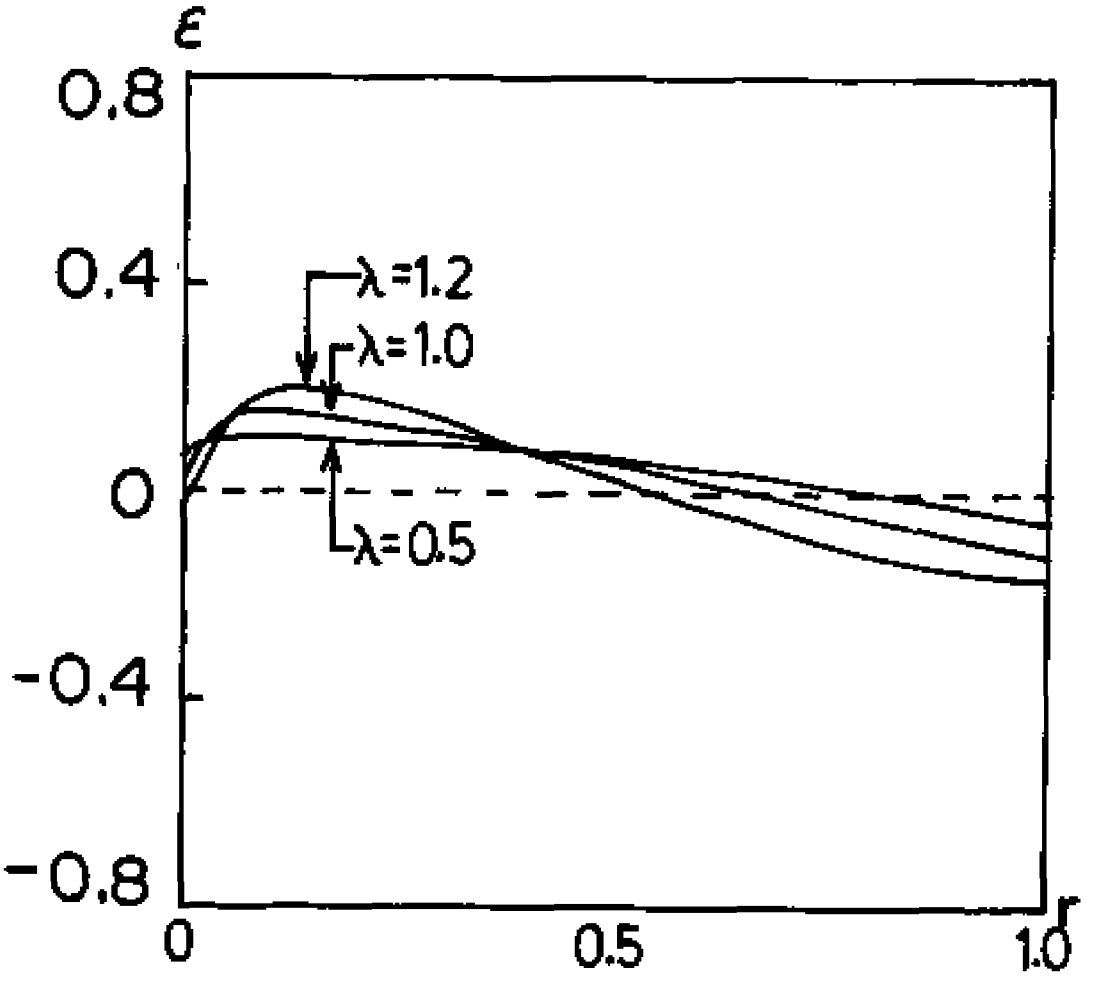

Fig. 8. The local relative deviation ε(r) of numerically computed solutions from force-free states for linearized most probable state equations of the second type (Eqs. (111) and (112)).

G. Numerical Solutions in the Tokamak Regime

We turn now to consideration of dimensionless flux and current values appropriate to tokamaks. Since the toroidal magnetic field and current in a tokamak are known to be non-negative functions of the radius, there is no problem in applying the methods of this chapter to find most probable tokamak equilibria. To arrive at the appropriate values of Φ and I we use the basic parameters from the PLT device[24] which has a minor radius of a = 0.4m, an average toroidal field of B_T = 3.5 Telsa, and a current $\sim$0.54 MA. Taking $B_o \sim B_T$ one finds $\Phi \sim .5$ and $I \sim .05$. Similar values are found for other tokamaks.

A survey of solutions for these values of flux and current reveal much the same behavior as in the case of $\Phi = I = 1$. The major difference, as a result of the boundary conditions imposed in this case, is that $B_z >> B_\theta$ which is the proper ordering for a tokamak. Because diamagnetic tokamaks (increasing B_z with r) having a current density peak on axis are often of particular interest we shall limit our discussion primarily to values of $\beta < 0$, and $\gamma < 0$ where these features are expected.

Figure (9) shows the behavior of the constants E and H in this quadrant. One feature that may be discerned from these plots is that the helicity has a much greater range of variation ($\sim$250% of the minimum value) than the energy ($\sim$66%) in the same region of the $\beta - \gamma$ plane. This is because the major contribution to the energy is from the B_z

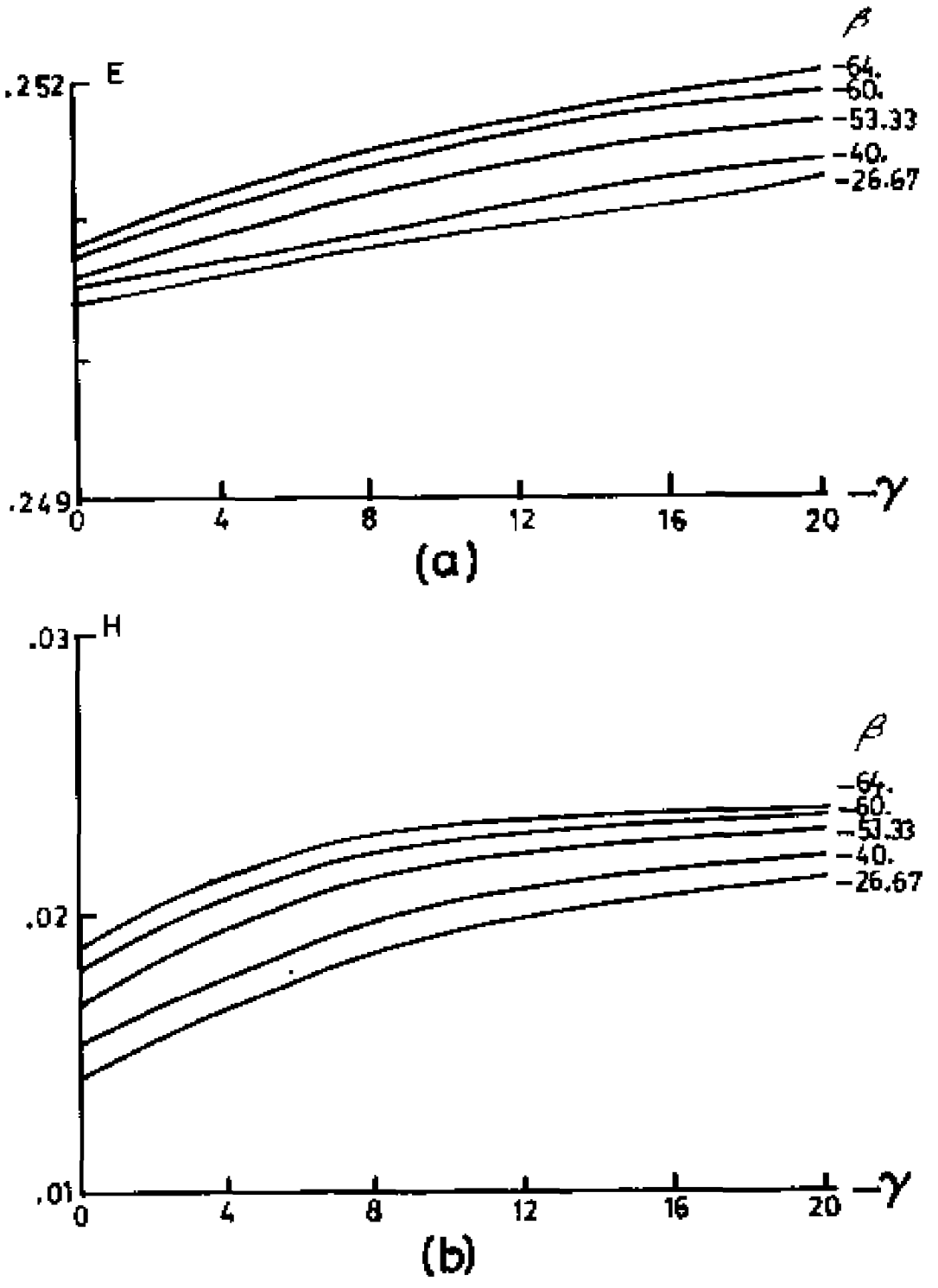

Fig. 9. Dependence of energy (a) and magnetic helicity (b) on β and γ for $\Phi = 0.5$, and $I = 0.05$, when $\beta < 0$, and $\gamma > 0$.

field which, as will be seen in specific examples, has a very gentle gradient in this flux-current regime.

As an example of the influence of the constants E and H on solutions we first present in Fig. (10), three profiles with fixed helicity (H = .0227) and decreasing energy. The major effect is a sharp drop in the equilibrium pressure as the energy is lowered. The B_z profile tends to flatten and the peak B_θ decreases. Because of these changes in the profiles the plasma beta drops dramatically from $\beta_{pl} = 0.47$ in profile (a) to $\beta_{pl} = 0.08$ in profile (c). The change in energy is only -0.2%. Since the poloidal field component is the most influential with respect to confinement in tokamaks, it is of some interest to note the change in the poloidal beta, where

$$\beta_{pol} \quad \frac{2\ p(o)}{(B_{\theta\ max})^2} \tag{158}$$

As the energy decreases β_{pol} changes from $\beta_{pol} = 21.8$ in (a) to $\beta_{pol} = 6.05$ in (c).

In the second example, shown in Fig. (11), the energy is held fixed at E = .2522 and the magnetic helicity is increased. A change in helicity of 2.5% from H = 0.2334 to H = .02394 causes changes in the profiles which are similar to those in which E is decreased relative to fixed H. The B_z field flattens while there is an increase in the maximum B_θ when H is increased (E fixed) as opposed to a decrease when E is lowered (H fixed). The drop in pressure and the flattening

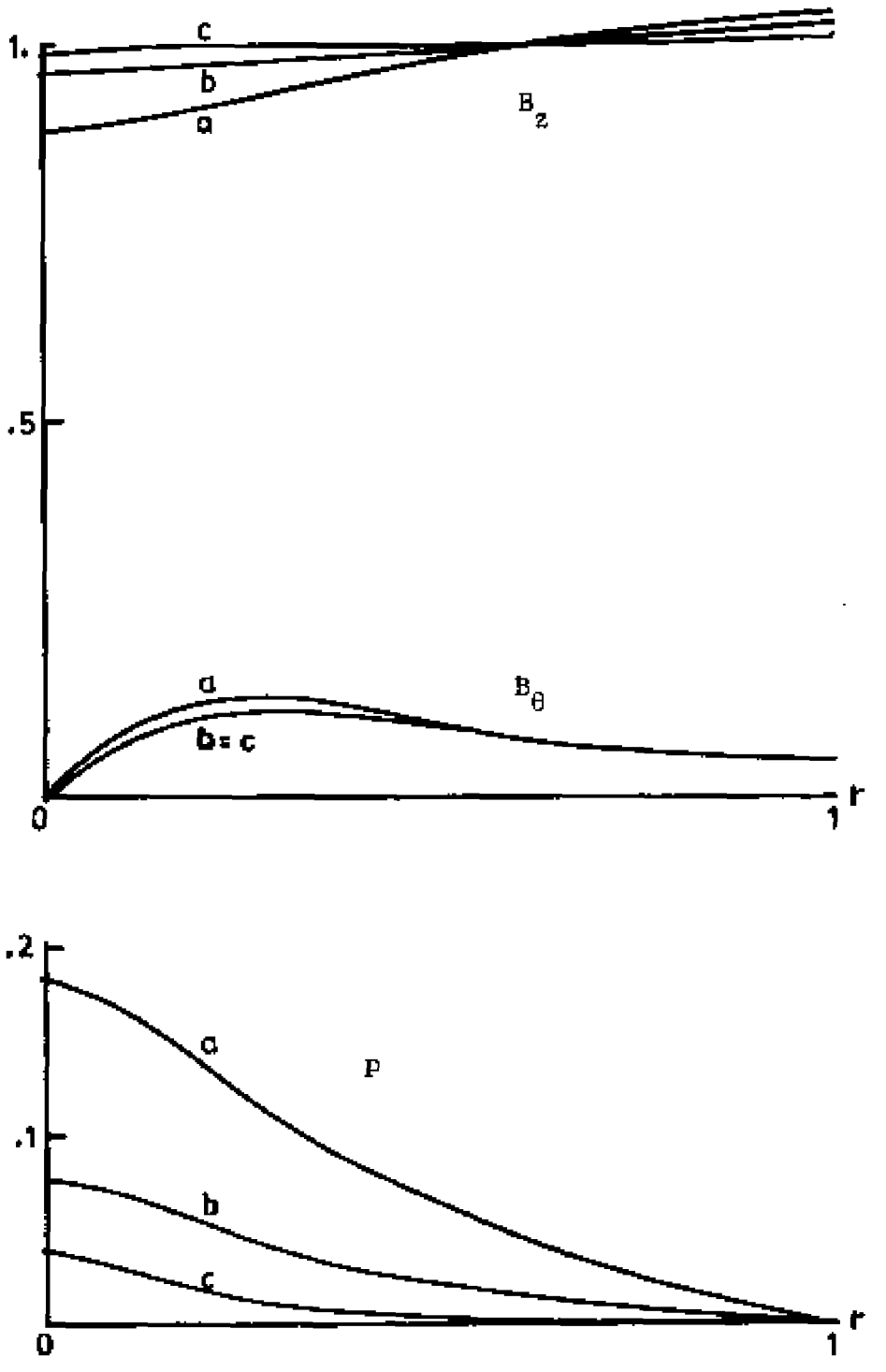

Fig. 10. Most probable equilibria in the tokamak regime with fixed helicity (H = 0.0227) and decreasing energy: (a) E = 0.2520, β_{pl} = 0.466; (b) E = 0.2516, β_{pl} = 0.167; (c) E = 0.2515, β_{pl} = 0.08.

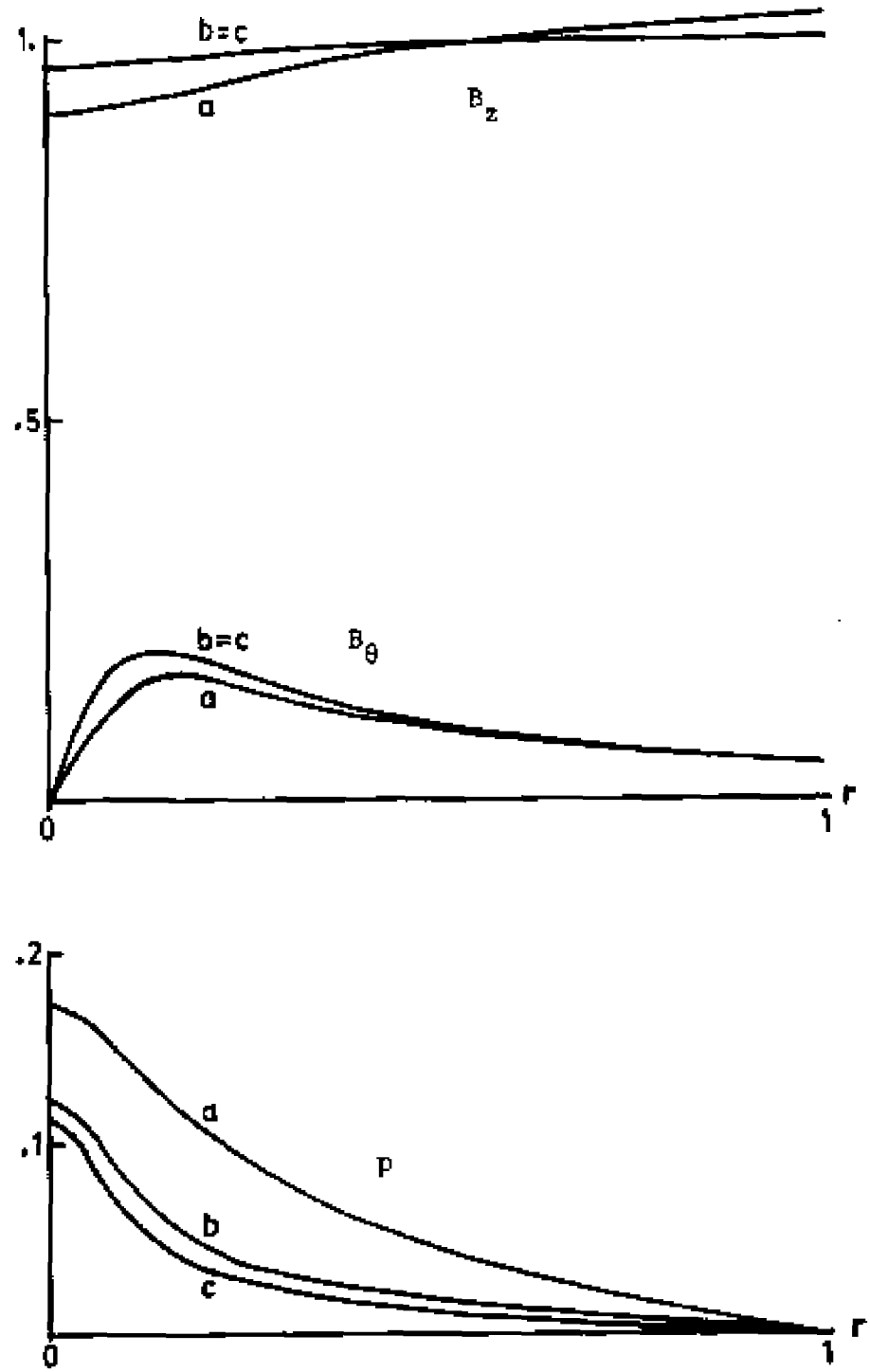

Fig. 11. Most probable equilibria in the tokamak regime with fixed energy (E = 0.2522) and increasing helicity: (a) H = 0.02334, β_{pl} = 0.427; (b) H = 0.02388, β_{pl} = 0.272; (c) H = 0.02394, β_{pl} = 0.243.

B_z profile cause a lowering of the plasma beta from $\beta_{pl} = 0.427$ in profile (a) to $\beta_{pl} = 0.243$ in profile (c). The poloidal beta is also lessened from $\beta_{pol} = 12.6$ to $\beta_{pol} = 6.0$. Thus the general tendency would seem to be a marked decrease of β_{pl} and β_{pol} as the ratio E/H decreases. It is impossible, of course, to adequately assess the effects on stability without performing a proper analysis of the growth rates of perturbations to these equilibria. However a rough estimate is that equilibria with higher β_{pl} and β_{pol} are apt to be more unstable. Therefore, the expectation is that a decrease in the energy-to-helicity ratio is likely to lead to more stable configurations.

III. REVERSED-FIELD PINCH CONFIGURATIONS AS MOST PROBABLE STATES

A. Extension of the Most Probable State Model to Reversed Magnetic Fields

To apply the methods of Chapt. II while allowing the possibility that the random field $B_z(r)$ is negative, one must arrive at a measure of the entropy for possible realizations of the system. However, the Boltzmann counting method of Chapt. II is only valid for non negative random functions. Following a suggestion by Montgomery[6] we present in this chapter an extension of the procedure discussed in Chapt. II for the purpose of estimating the most probable equilibria for a reversed-field pinch.

The starting point is a decomposition of the random B_z function into two random parts,

$$B_z = B_z^+ - B_z^- \tag{159}$$

where B_z^+ and B_z^- are non negative independent functions with integrals

$$\phi^+ = \int_0^1 B_z^+(r) r dr \tag{160}$$

$$\phi^- = \int_0^1 B_z^-(r) r dr \tag{161}$$

The total flux $\phi = \phi^+ - \phi^-$ is to be imposed as a physical constraint. Using the Boltzmann counting method as before, and characterizing the possible realization of B_z^+ and B_z^- by the occupation numbers N_i^{B+}, and N_i^{B-}, the expression for the entropy associated with the B_z field is

$$\ln W_B = - \sum_i N_i^{B+} \ln \left(\frac{N_i^{B^+}}{N^{B^+}\Delta_i} \right) - \sum_i N_i^{B^-} \ln \left(\frac{N_i^{B^-}}{N^{B^-}\Delta_i} \right) \tag{162}$$

We again impose the constraints I, E, and H in addition to ϕ. After maximizing the total entropy subject to these constraints one obtains the continuum expressions

$$B_z^+ = \phi^+ \exp\left(-\alpha_B - \beta B_z - \gamma A_z\right) \tag{163}$$

$$B_z^- = \phi^- \exp\left(\alpha_B + \beta B_z + \gamma A_z\right) \tag{164}$$

The field B_z is then the difference of these expressions. Since the J_z current profiles of both reversed-field pinches and tokamaks are experimentally observed to be non negative functions, we have not extended the formulation to allow reversal of J_z and thus the equation for the most probable J_z is unchanged. We then have the system of equations

$$B_z = \phi^+ \exp(-\alpha_B - \beta B_z - \gamma A_z) - \phi^- \exp(\alpha_B + \beta B_z + \gamma A_z) \tag{165}$$

$$J_z = \exp(-\alpha_J - \beta A_z - \gamma \Pi) \tag{166}$$

$$\Pi''(r) + \frac{1}{r}\Pi'(r) = -B_z(r) \tag{167}$$

$$A_z''(r) + \frac{1}{r}A_z'(r) = -J_z(r) \tag{168}$$

with

$$\phi^- = \phi^+ - \Phi \tag{169}$$

and

$$A_z(1) = \Pi(1) = 0 \tag{170}$$

for the most probable profiles.

ϕ^+ is a free parameter in this formulation. Its presence in the final equation indicates a possible dependence of the solutions on an arbitrary decomposition of the physical field. To fix this parameter we must again examine the entropy, for one must choose the most probable state from the largest class of possible realizations compatible with the given information. Therefore the entropy must be maximal not only with respect to the constraints, but with respect to the decomposition as well.

The entropy in the continuum limit may be written as

$$S = -\int r dr\, B_z^+ \ln\left(\frac{B_z^+}{\phi^+}\right) - \int r dr\, B_z^- \ln\left(\frac{B_z^-}{\phi^-}\right) - \int r dr\, J_z \ln\left(\frac{J_z}{I}\right) \tag{171}$$

Upon substitution B_z^+, B_z^-, and J_z, from Eqs. (165) and (166) integration of Eq. (171) yields

$$S = \alpha_B \phi + \alpha_J I + 2\beta E + \gamma H \tag{172}$$

For fixed constraints Φ, I, E, and H, a variation in ϕ^+ can only change the entropy through the Lagrange multipliers α_B, α_J, β, and γ.

To examine the behavior of the entropy with changing Φ^+, let us first consider a simple case for which there are analytic solutions. Setting $\gamma = 0$ (unconstrained helicity) one obtains solutions of Chapt. II, Sec. B.

$$B_z = 2\Phi^+ \sinh(-\alpha_B - 2B\Phi) + \Phi\, e^{\alpha_B + 2B\Phi} = 2\Phi \tag{173}$$

$$J_z = \exp(-\alpha_J - BA_z) \tag{174}$$

$$A_z = \frac{-2}{B} \ln\left| (B+1) \,/\, (Br^2+1) \right| \tag{175}$$

with

$$B = -\frac{4B}{(B+1)\,I} \quad ; \quad e^{\alpha_J} = \frac{(B+1)}{2I} \tag{176}$$

The energy as in Chapt. II is

$$E = 2\Phi^2 + \frac{4}{B^2}\left| \ln(1+B) - B\,(B+1)^{-1} \right| \tag{177}$$

The ratio

$$\frac{(2E - 4\Phi^2)}{I^2} = \frac{2(1+B)^2}{B^2}\left| \ln(1+B) \;\; \frac{-B}{(B+1)} \right| \tag{178}$$

depends only on the parameter B which, for given Φ and I, fixes the

value of the energy. The parameter α_B is determined by specification of the decomposition ϕ^+ and the flux ϕ in Eq. (173). To find the dependence of α_B on ϕ^+ we let

$$Z = e^{-\alpha_B - 2\beta\phi} \tag{179}$$

which by Eq. (174) gives

$$Z^2\phi^+ - 2Z\phi - (\phi^+ - \phi) = 0 \tag{180}$$

Solving for Z,

$$Z = \frac{1}{\phi^+}\left[\phi + \sqrt{\phi^2 + \phi^+(\phi^+ - \phi)}\right] \tag{181}$$

and thus from the definition Eq. (179)

$$\alpha_B = \ln\phi^+ - \ln\left[\phi + \sqrt{\phi^2 + \phi^+(\phi^+ - \phi)}\right] - 2\beta\phi \tag{182}$$

Since the Lagrange multipliers α_J and β are fixed by the constraints, the entropy

$$S = \alpha_B(\phi^+)\phi + \alpha_J I + 2\beta E \tag{183}$$

is a linear function only of $\alpha_B(\phi^+)$. From Eq. (182) α_B is a mono-

tonically increasing function of ϕ^+ with an asymptotic limit of

$$\lim_{\phi^+ \to \infty} \alpha_B(\phi^+) = -2\beta\phi \tag{184}$$

Thus the entropy is asymptotic in Φ^+. A plot of S, for the special case in which $\phi = I = B = 1$, is shown in Fig. (12). This simple example illustrates an asymptotic trend in the entropy as a function of the decomposition parameter Φ^+. In this case the solutions are invariant with respect to ϕ^+ for fixed constraints, as B_z is already determined to be a constant for arbitrary Φ^+. However, when $\gamma \neq 0$, B_z as well as other functions may well depend on the decomposition. For the full problem then ($\gamma \neq 0$), we must develop some criterion for selecting a decomposition which is consistent with our search for the maximum entropy configuration.

The solutions for $\gamma \neq 0$ must be found numerically as in Chapt. II. Our procedure is to follow several solutions from $\Phi^+ = \phi$ to $\phi^+ >> \phi$ holding ϕ, I, E, and H fixed by adjustment of all four Lagrange multipliers while calculating the entropy from Eq. (172) at each step. The dimensionless current and flux values $\phi = 0.1$, $I = .15$ which were chosen for these computations were derived from the maximum field and current specifications of an experimental reversed-field pinch (HBTX-1),[20] in which $B_o \sim 1$ Tesla, a = 6.5 cm, and the current is 55 kA.

Figure (13) shows two such runs for fixed E and H. Note the dependence of the Lagrange multipliers on the ratio Φ^+ / ϕ. The

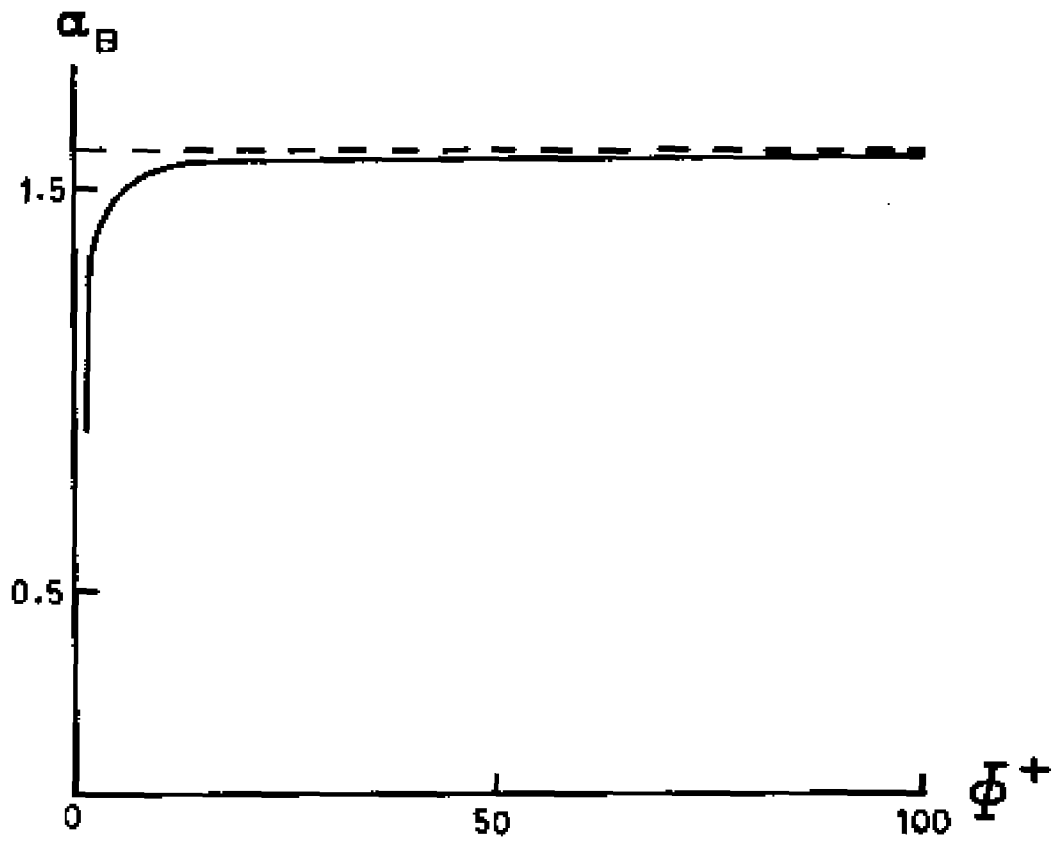

Fig. 12. α_B as a function of Φ^+ for unconstrained helicity ($\gamma = 0$) when $\Phi = 1$, $I = 1$, and $B = 1$.

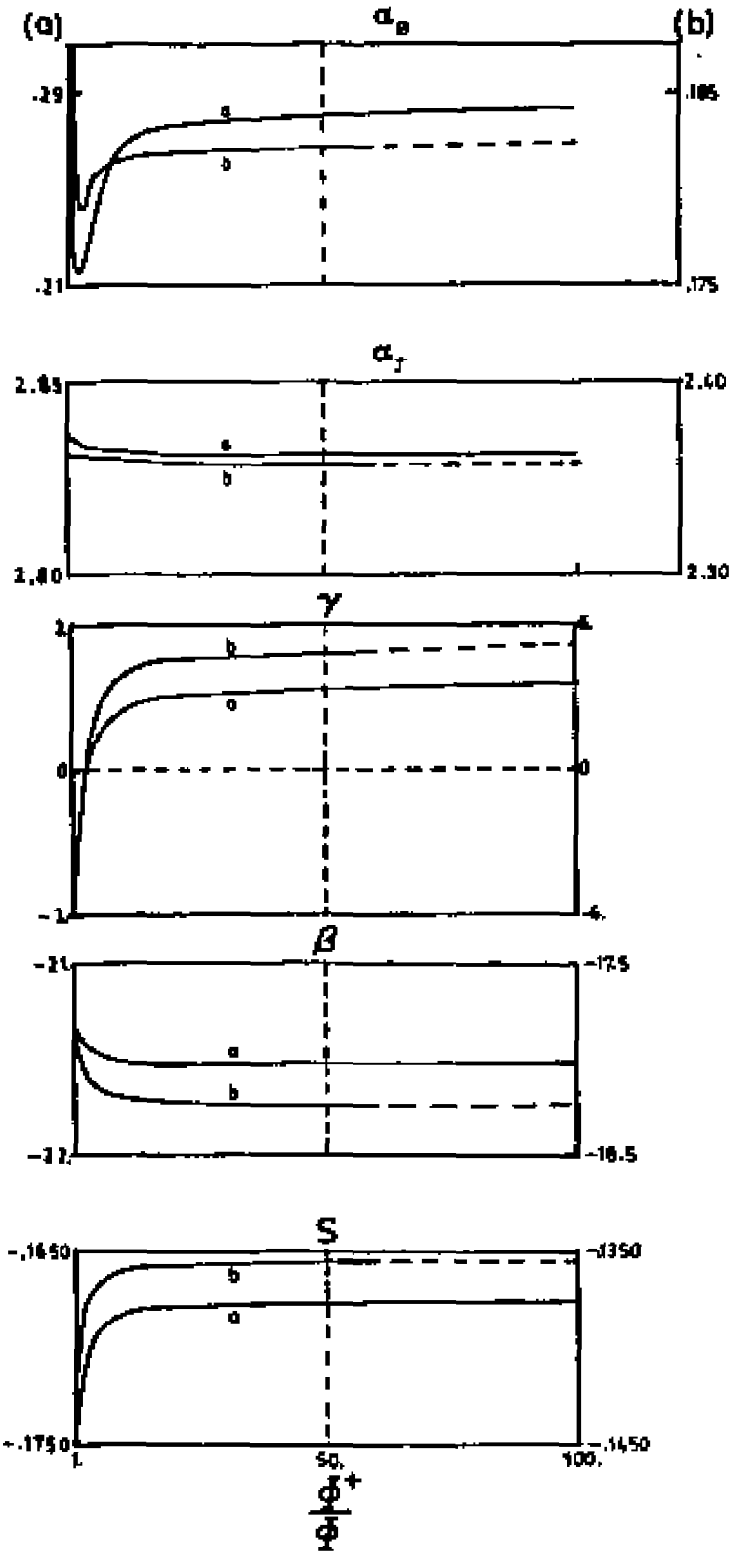

Fig. 13. Dependence of the Lagrange multipliers α_B, α_J, β, and γ; and the entropy S on Φ^+ when $\gamma \neq 0$.

multipliers α_J and β approach constant values quickly, while α_B and γ level off more slowly. The entropy rises sharply and seems to become asymptotic for large Φ^+. As Φ^+ / Φ becomes large, the solutions tend to an asymptotic form as a result of the continuing readjustment of the multipliers required to hold to fixed constraints. The change in B_z as Φ^+ increased is shown in Fig. (14), for run (a).

The vertical broken line in Fig. (13) marks a special value Φ_s^+ / Φ for which the equation for B_z takes on a particularly simple form. Writing Eq. (165) as

$$B_z = \frac{1}{2}\left[\exp\left(\ln 2\Phi^+ - \alpha_B - \eta\right) - \exp\left(\ln 2\Phi^- + \alpha_B + \eta\right)\right] \tag{185}$$

where $\eta = \beta B_z + \gamma A_z$, suggests defining a new parameter

$$\alpha_B^* = \alpha_B - \ln 2\Phi_s^+ = \alpha_B + \ln 2\Phi_s^- \tag{186}$$

for which the right hand side of Eq. (186) becomes a hyperbolic sine function. Equation (187) imposes on Φ_s^+ and Φ_s^- the relation

$$\Phi_s^+ = 1/4\Phi_s^- \tag{187}$$

Taking into account the constraint $\Phi_s^+ - \Phi_s^- = \Phi$ one obtains

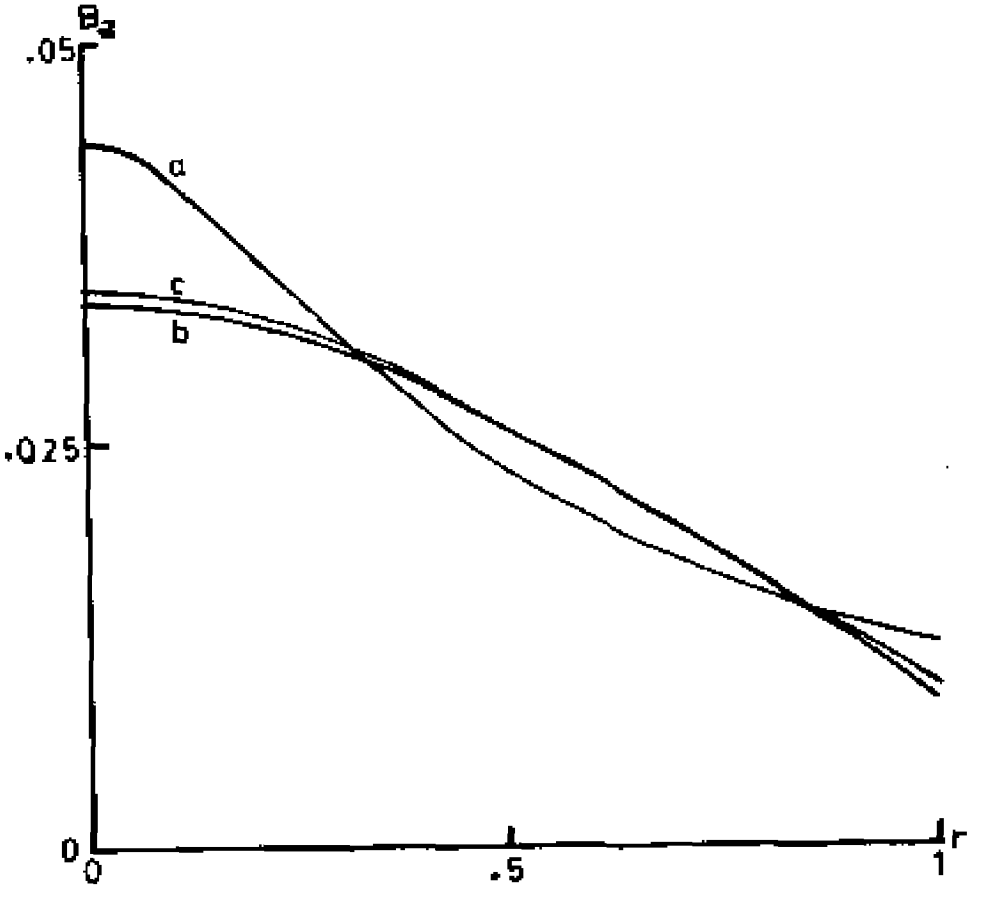

Fig. 14. Asymptotic behavior of the B_z profile with Φ^+: (a) $\Phi^+ = \Phi$, (b) $\Phi^+ = 4\Phi$, (c) $\Phi^+ = 10\Phi$ through $\Phi^+ = 60\Phi$. For these solutions $\Phi = 0.01$, $I = 0.15$, $E = 0.00568$, and $H = 0.001263$ corresponding to numerical run (b) of Fig. 13.

$$\phi^+_s = \frac{1}{2}\left(\phi + \sqrt{\phi^2 + 1}\right) \tag{188}$$

Thus for a given Φ there is a special value ϕ^+_s for which Eq. (185) becomes

$$B_z = \sinh\left(-\alpha_B^* - \beta B_z - \gamma A_z\right) \tag{189}$$

A plot of ϕ^+_s / ϕ vs Φ in Fig. (15) shows that for small values of ϕ, $\phi^+_s >> \phi$ while for larger ones $\phi^+_s \sim \phi$. Our choice of $\phi = .01$ implies $\phi^+_s / \phi \sim 50$, thereby placing the sinh-equation solutions well into the asymptotic region. The apparent asymptotic tendency of the entropy with ϕ^+, the position of the sinh-equation solutions in the asymptotic region (for small Φ), and the convenience of using Eq. (189) instead of Eq. (165) for numerical computation leads us to adopt the following convention. For the reversed-field case we will demand that $\Phi \sim .01$ (which can be kept small by redefining the characteristic field strength B_o if necessary). Estimates of the most probable state are then to be found using the sinh-form of B_z Eq. (189).

B. Most Probable States in the Reversed-Field Pinch Regime

Solutions to the most probable state equations were found with B_z given by Eq. (189), and with $\Phi = .01$ and $I = 1.5$. The qualitative appearance of the solutions can again be related to the position of the

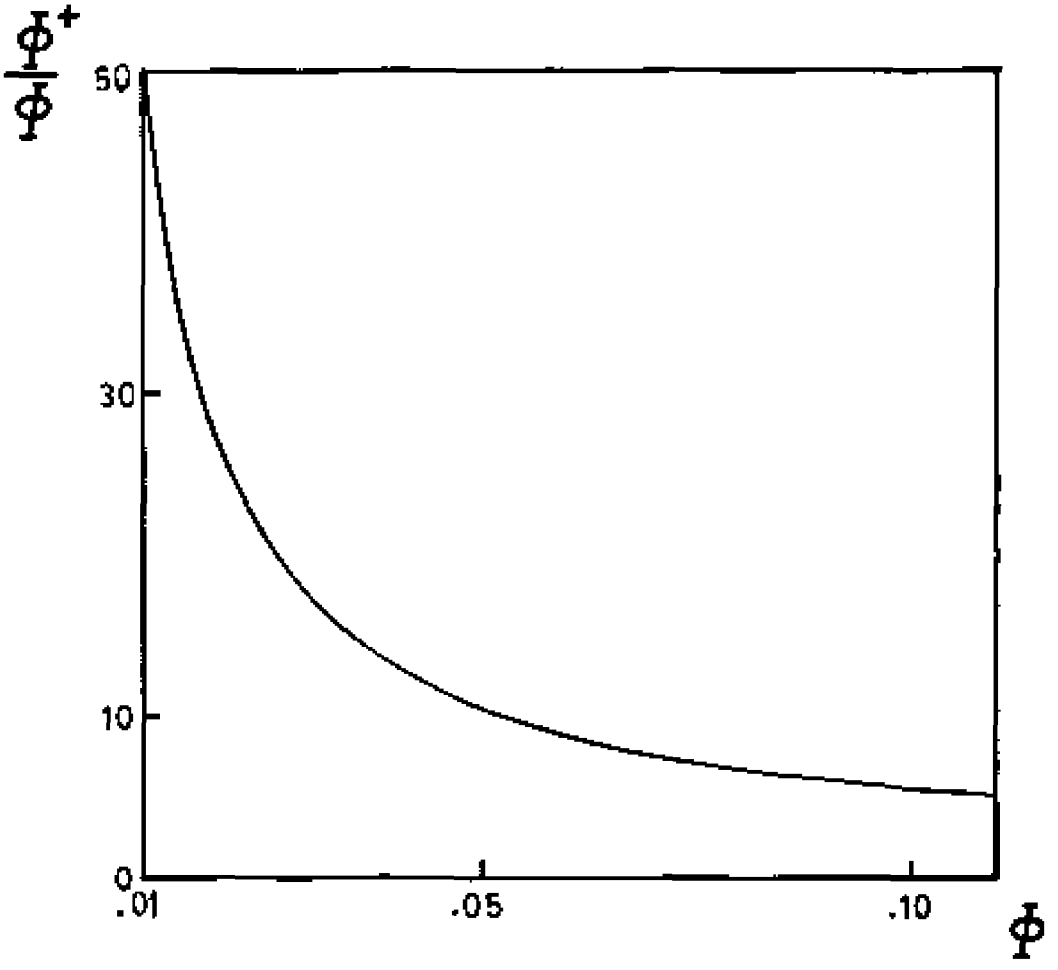

Fig. 15. Dependence of the ratio Φ_3^+/Φ on the constraint Φ.

point (β, γ) in the β - γ parameter plane. Beginning with $\beta < 0$, $\gamma > 0$ as in Fig. (16(a)) one finds a reversed field B_z for sufficiently large γ with $B_z(0) > 0$ and $B_z(1) < 0$. J_z is peaked on axis falling to a small value at $r = 1$. As γ is decreased at fixed β, the reversal disappears and B_z flattens, becoming constant at $\gamma = 0$. Decreasing γ still further causes $B_z(0)$ to become smaller until for sufficiently small γ, B_z is again a reversed field but with the opposite sense as shown in Fig.(16(b)) . J_z remains qualitatively the same as γ decreases. In the opposite quadrant where $\beta > 0$ and $\gamma > 0$, B_z in Fig. (17(a)) is reversed with $B_z(0) < 0$. J_z is peaked at the wall. Lowering γ causes loss of the reversal as B_z flattens to a constant, and then for $\gamma < 0$, B_z again reverses with $B_z(1) < 0$ as in Fig. (17(b)). J_z retains its skin current appearance. Intermediate of these two trends are the solutions for unconstrained energy ($\beta = 0$). The profiles (Fig. (18)) show that these solutions for B_z are much the same as for $\beta > 0$ but with J_z peaked on axis as for $\beta < 0$.

Experimental measurement of field profiles using probes suggest that reversed-field pinch profiles commonly resemble those of Fig. (16(a)), where $B_z > 0$ on axis and J_z is peaked in the interior, or those of Fig. (16(b)) where B_z has the opposite sense. Theoretical models usually assume that $B_z(0) > 0$. We therefore restrict our investigations to solutions with $\beta < 0$, $\gamma > 0$.

A plot of the energy and helicity vs. γ is shown for this region in Fig. (19). With the help of these curves the effect of the

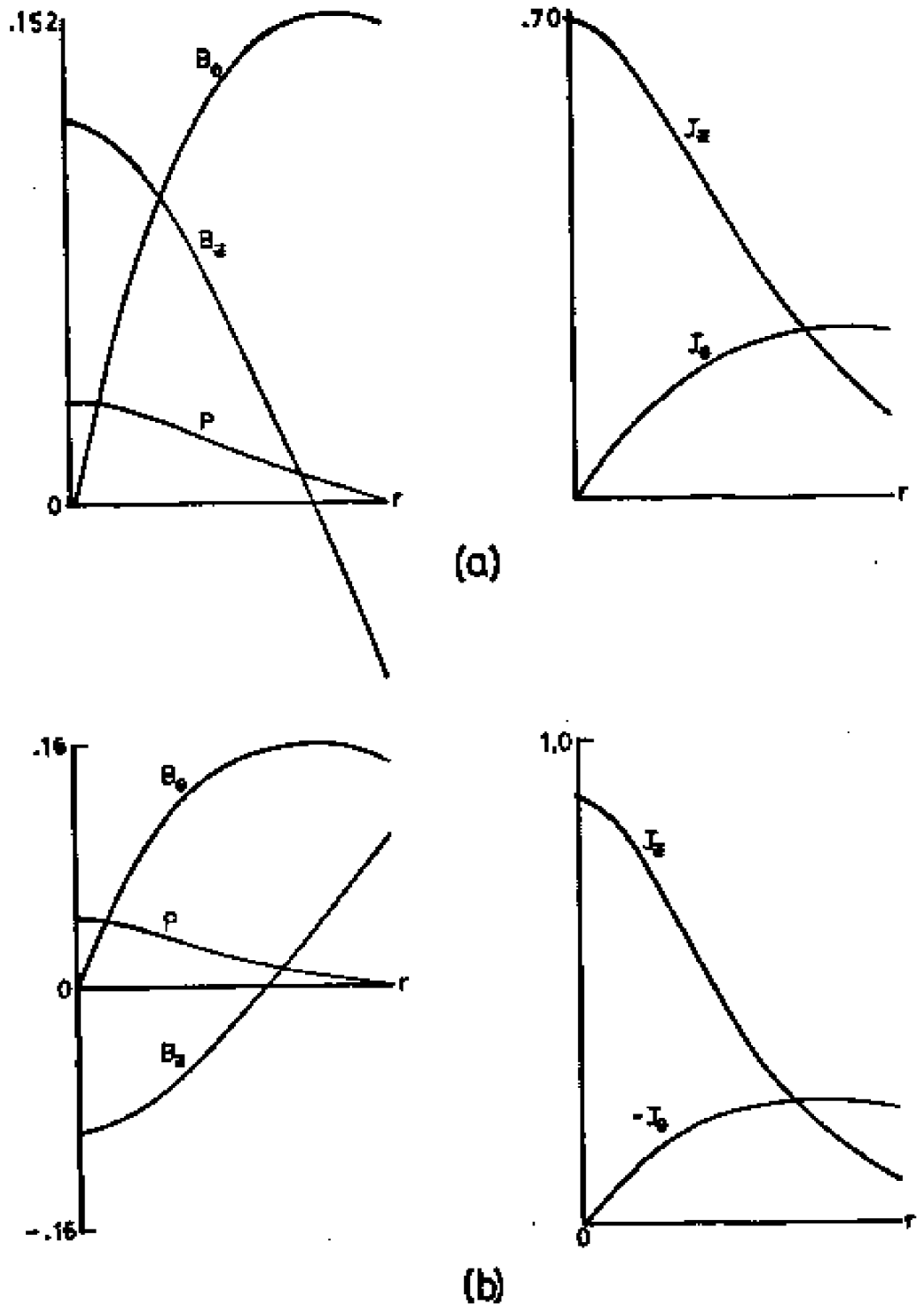

Fig. 16. Most probable reverse field equilibria when (a) $\beta < 0$, and $\gamma > 0$; (b) $\beta < 0$, and $\gamma < 0$.

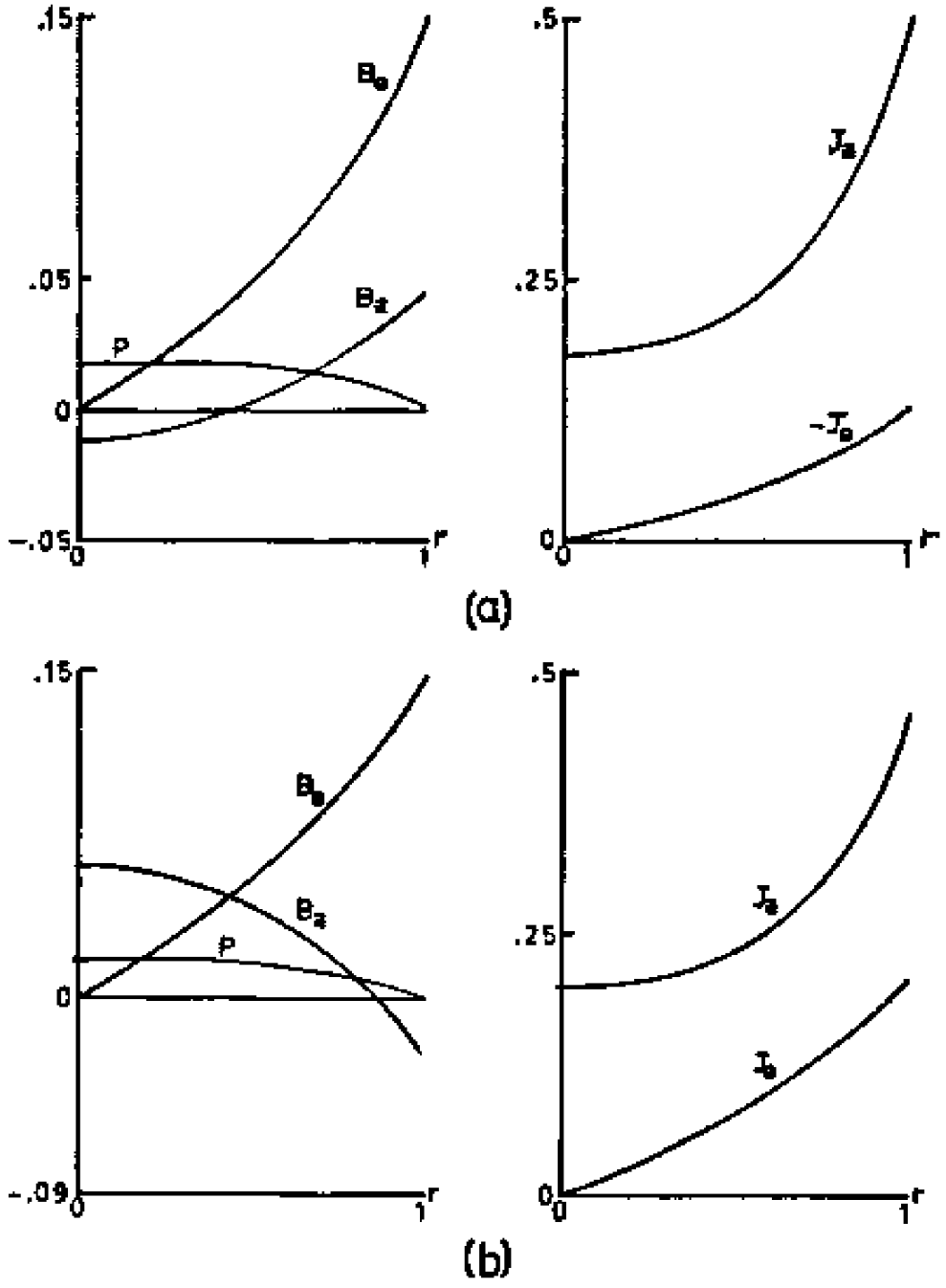

Fig. 17. Most probable reverse field equilibria when (a) $\beta > 0$, and $\gamma > 0$; (b) when $\beta > 0$ and $\gamma < 0$.

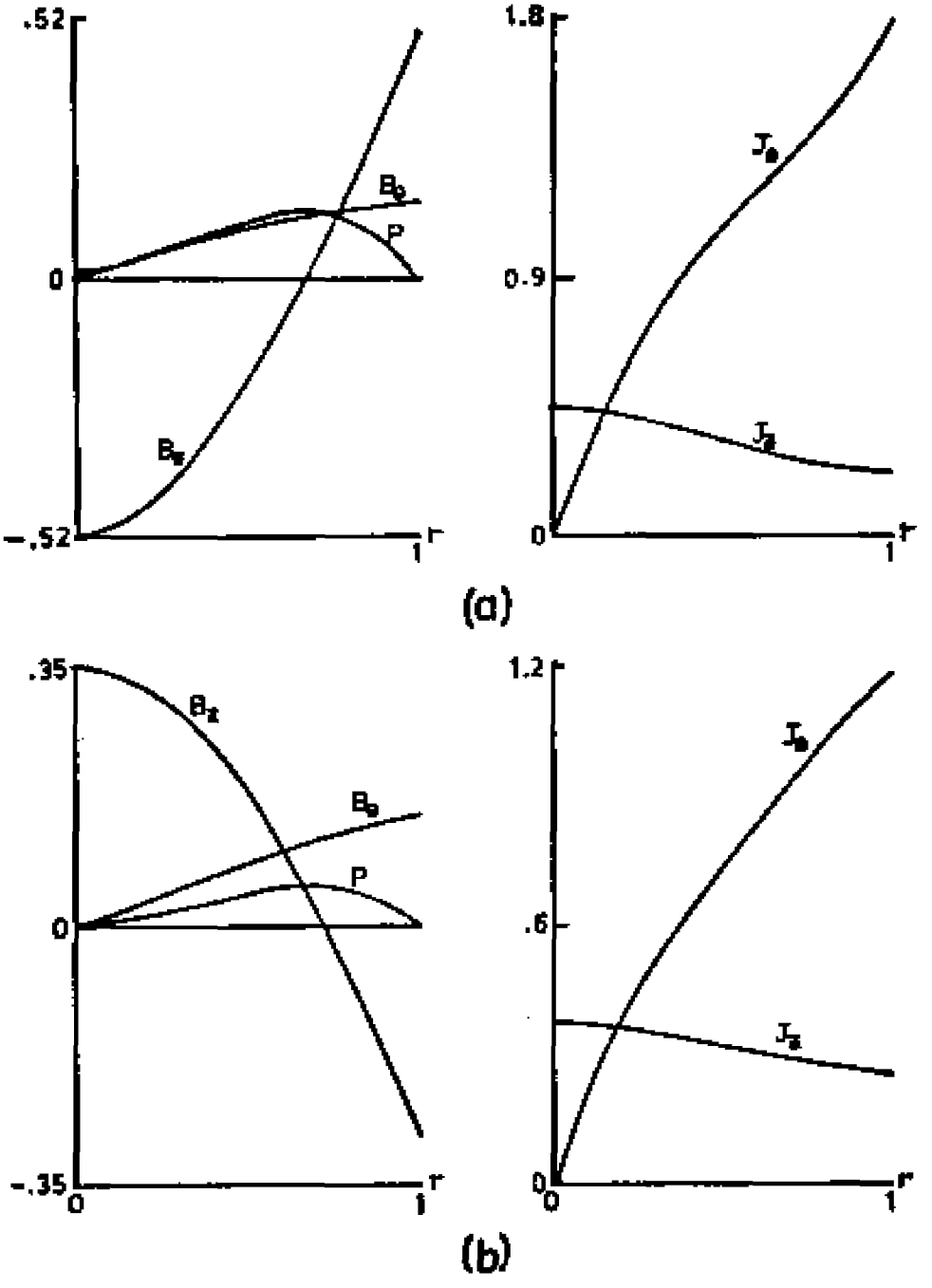

Fig. 1ß. Most probable reverse field equilibria when (a) $\beta = 0$, and $\gamma > 0$; (b) $\beta = 0$ and $\gamma < 0$.

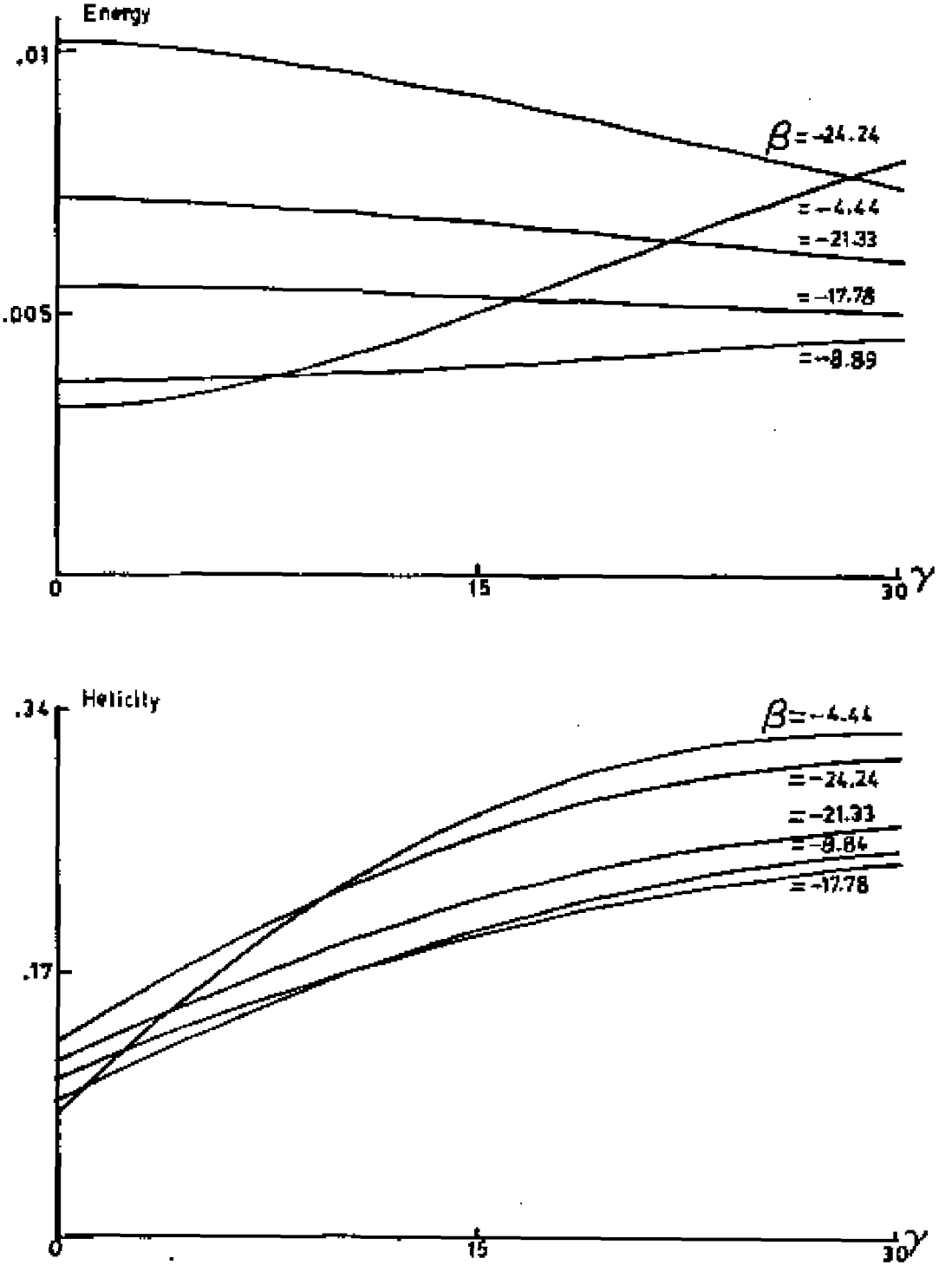

Fig. 19. Energy (a) and magnetic helicity (b) versus γ for various β in the reverse field pinch regime.

energy on the equilibria at fixed helicity may be investigated. Taking H = .002 arbitrarily, one finds four solutions in Fig. (19) with different energies for various values of β and γ. These profiles are plotted in Fig. (20) The solution with the highest energy (E = .0098) has a non-reversed B_z profile and a sharply peaked B_θ field. As the energy is decreased to E = .0068, reversal sets in, B_0 flattens somewhat, and the pressure on axis drops. The development of a stronger reversed field continues as the energy decreases with respect to fixed magnetic helicity H. The plasma beta β_{pl} decreases as the energy is lowered as a result of the lowered pressure and the incressed field on axis. Eventually the pressure profile becomes hollow. Following other solutions at fixed H in the same way suggests this trend is quite consistent. These features are compatible with the notion that self-reveraal occurs as the energy is lowered at fixed helicity. The decrease in β_{pl}, gives a possible indication that stability may be enhanced as a result of the lowered energy.

One may also examine the effects of increased helicity at fixed energy. Such a sequence for E = .006339 is plotted in Figs. (21). The main features as H increases are a drop in the pressure on axis (Fig. (21(B)), a more pronounced reversed field Fig. (21(a)) profile, and smaller values of B_θ in the interval (Fig. (21(b)) with a marked hollow pressure profile. These effects are quite similar to those encountered in lowering the energy with respect to a fixed helicity.

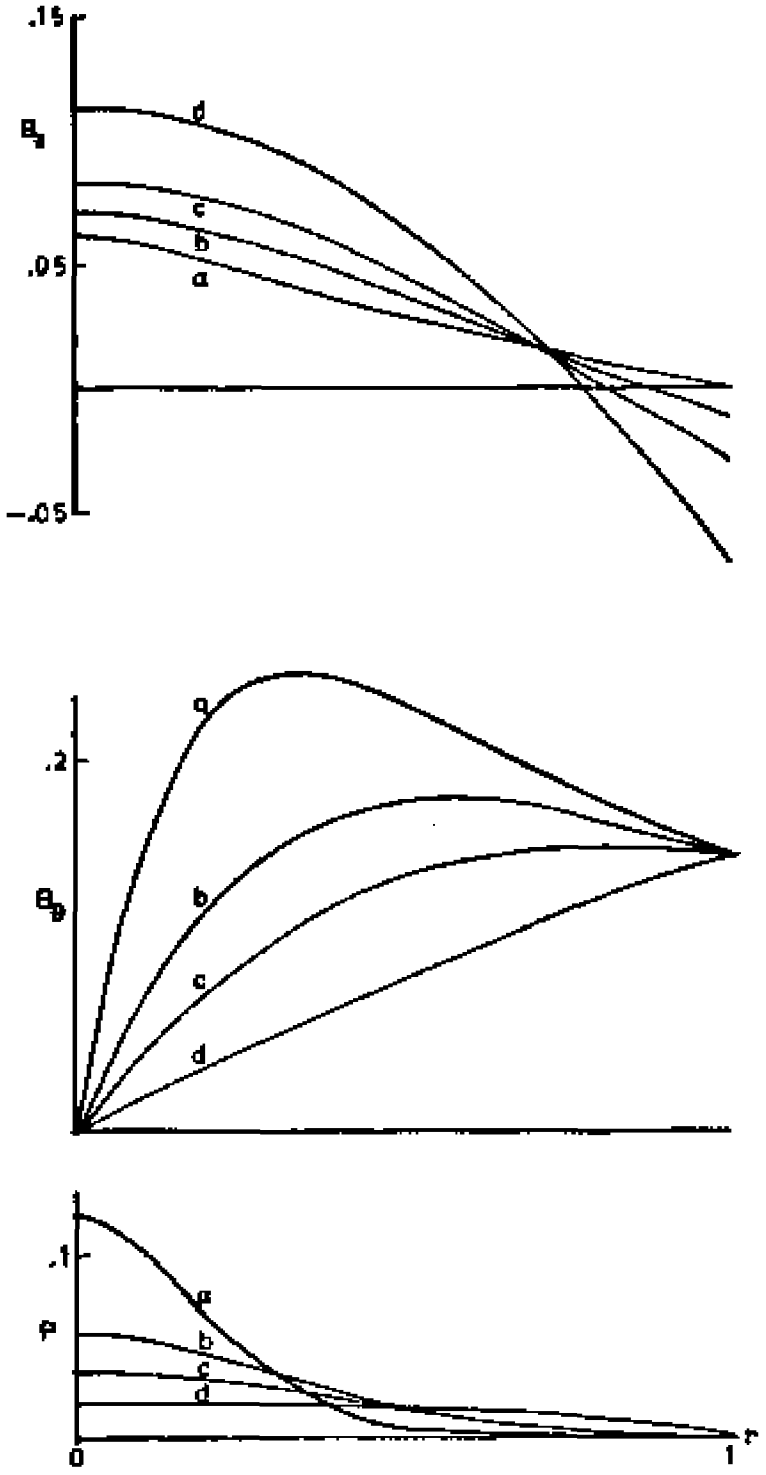

Fig. 20. Most probable reverse field pinch equilibria at fixed helicity with decreasing energy.

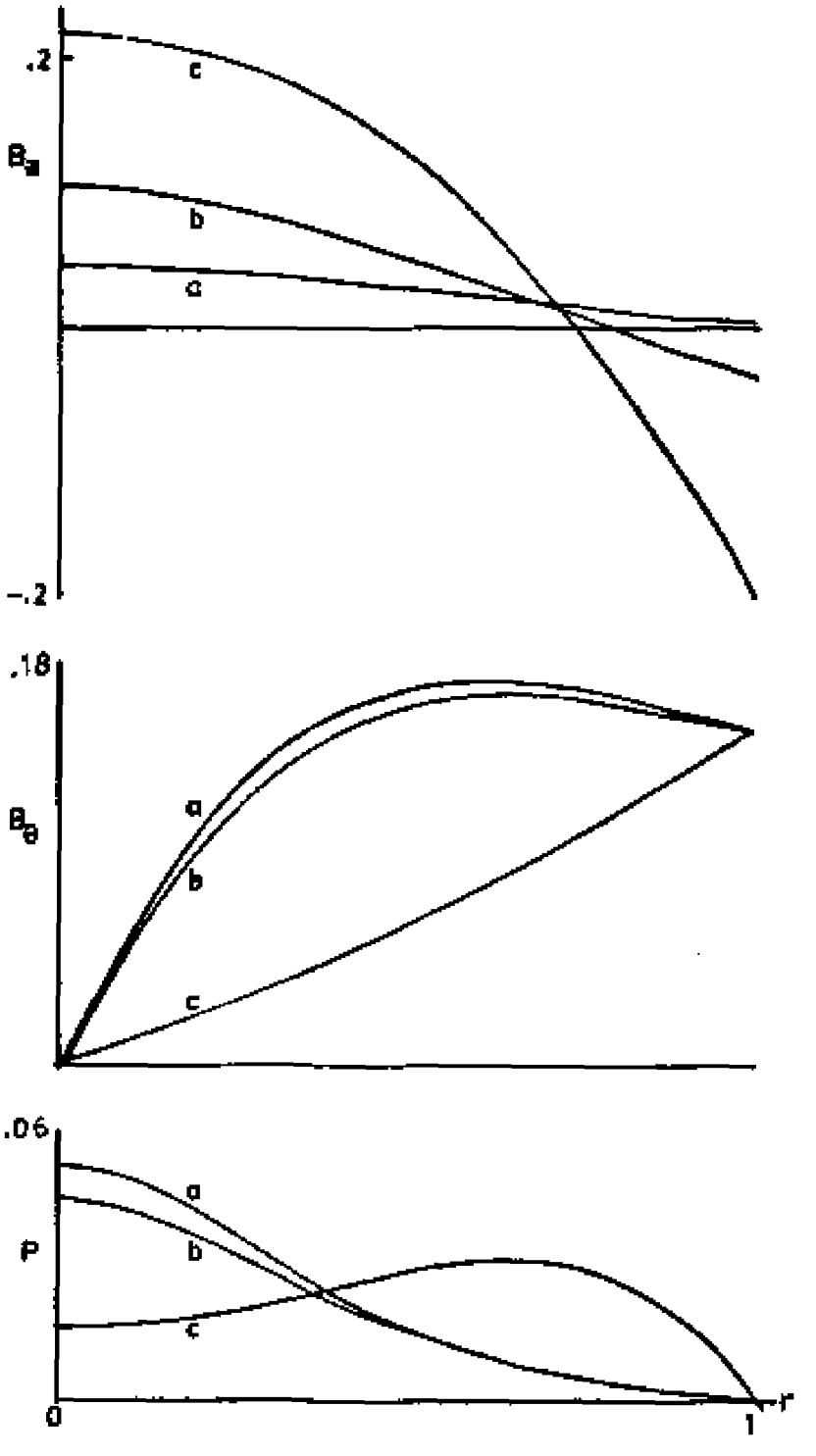

Fig. 21. Most probable reverse field pinch equilibria at fixed energy with increasing magnetic helicity.

On the basis of these observations and other numerical runs, it seems reasonable to conjecture that the process of self reversal at fixed flux and current is characterized by a decreasing energy to helicity ratio.

Finally we shall examine the dependence of most probable equilibria for the reversed-field pinch on the pinch ratio θ. In the preceeding solution θ was fixed at a large value of $\theta = 7.5$. Self-reversed experimental discharges seldom have a pinch ratio so large. Programmed reversed-field pinches are sometimes set up with $\theta \sim 7 - 8$, after which the ratio decays to a value of about 2. In order to make a proper comparison we note that the ratio

$$\mu_o \frac{I^* H^*}{E^* \Phi^*} \tag{190}$$

(where asterisks indicate that these are dimensional quantities) is a dimensionless number. The ratio can be split into two dimensionless factors

$$\mu_o \frac{I^* H^*}{E^* \Phi^*} = \mu_o \frac{I^* a}{2\Phi^*} \times \frac{2H^*}{aE^*} = \theta(a) \times \frac{2H^*}{aE^*} \tag{191}$$

Therefore a comparison of solutions will be made at a fixed energy-to-helicity ratio. The value of θ is varied by changing the current relative to a fixed toroidal flux. Four solutions with $\beta < 0$ and $\gamma > 0$

with E/H = 1.5 (dimensionless E and H) are presented in Fig. (22). At $\Theta = 4$ there is a rather large reversed field accompanied by a flattened and slightly hollow equilibrium pressure. As Θ is lowered to 3, the reversal point moves outward in radius, and the pressure changes to a monotone decreasing function. Decreasing Θ still further results in a non-reversed state at $\Theta = 2$. For $\Theta = 1$ the solution for B_z is nearly a constant. Further comparisons made at different energy-to-helicity ratios show a similar trend. Solutions at a smaller fixed value of E/H than those in Fig. (22) first exhibit field reversal at a lower value of Θ, while for large E/H the reversal first occurs at a higher Θ. To show this pattern more clearly we shall make use of a diagram which often appears in the reversed-field pinch literature.[18,19] In addition to the pinch ratio Θ one may define another dimensionless parameter

$$F = \frac{B_z^*(a)}{B_z^*\text{ average}} \tag{192}$$

where $B_z^*(a)$ is the value at the boundary (asterisks again denote physically measured quantities). In the present dimensionless units

$$F = \frac{B_z(1)}{2\Phi} \tag{193}$$

For a given Θ, F indicates the degree of reversal in a particular

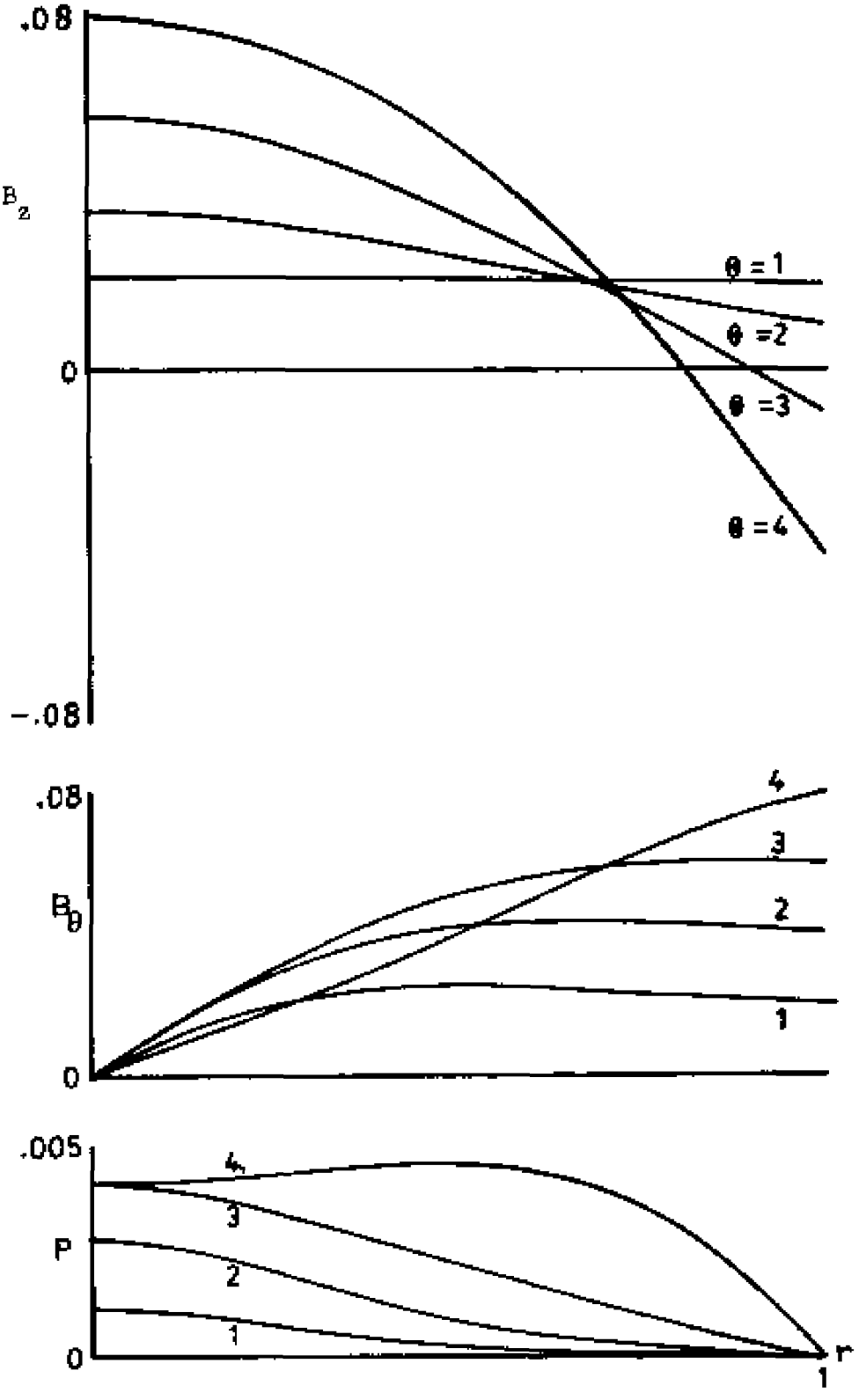

Fig. 22. Dependence of most probable reverse field equilibria on the pinch ratio Θ at fixed E/H.

discharge. Figure (23) is a diagram of F versus Θ for solution of the most probable state equations with various E/H. The solid curve represents the values of F and Θ which correspond to the analytic force-free solutions of Taylor's Bessel function model.[19] The values of E/H for these solutions are given in the legend of Fig. (23). One notices the tendency for increased reversal with increasing Θ for all cases. As E/H decreases, reversal occurs at progressively smaller values of Θ. In the present formulation of the most probable state equations, J_z is assumed to be non-negative, whereas the Bessel function force-free model demands that J_z be reversed when B_z is reversed, although such current profiles are not usually observed (this follows from $J_z(r) = \lambda B_z(r)$ in the Bessel function model). Therefore one cannot expect to find most probable reversed field equilibria which are force-free in this formulation.

As a final remark, it should be noted that reversed-field profiles with $\Theta = 2$ were found for sufficiently small E/H. However, no reversed field solutions were observed for $\Theta = 1.0$ despite an extensive search for such solutions within the $\beta - \gamma$ parameter space. This result is particularly interesting in light of predictions by Taylor[19] and others[18] which put the critical value of Θ for reversal in the range $1.2 \lesssim \Theta \lesssim 2.0$.

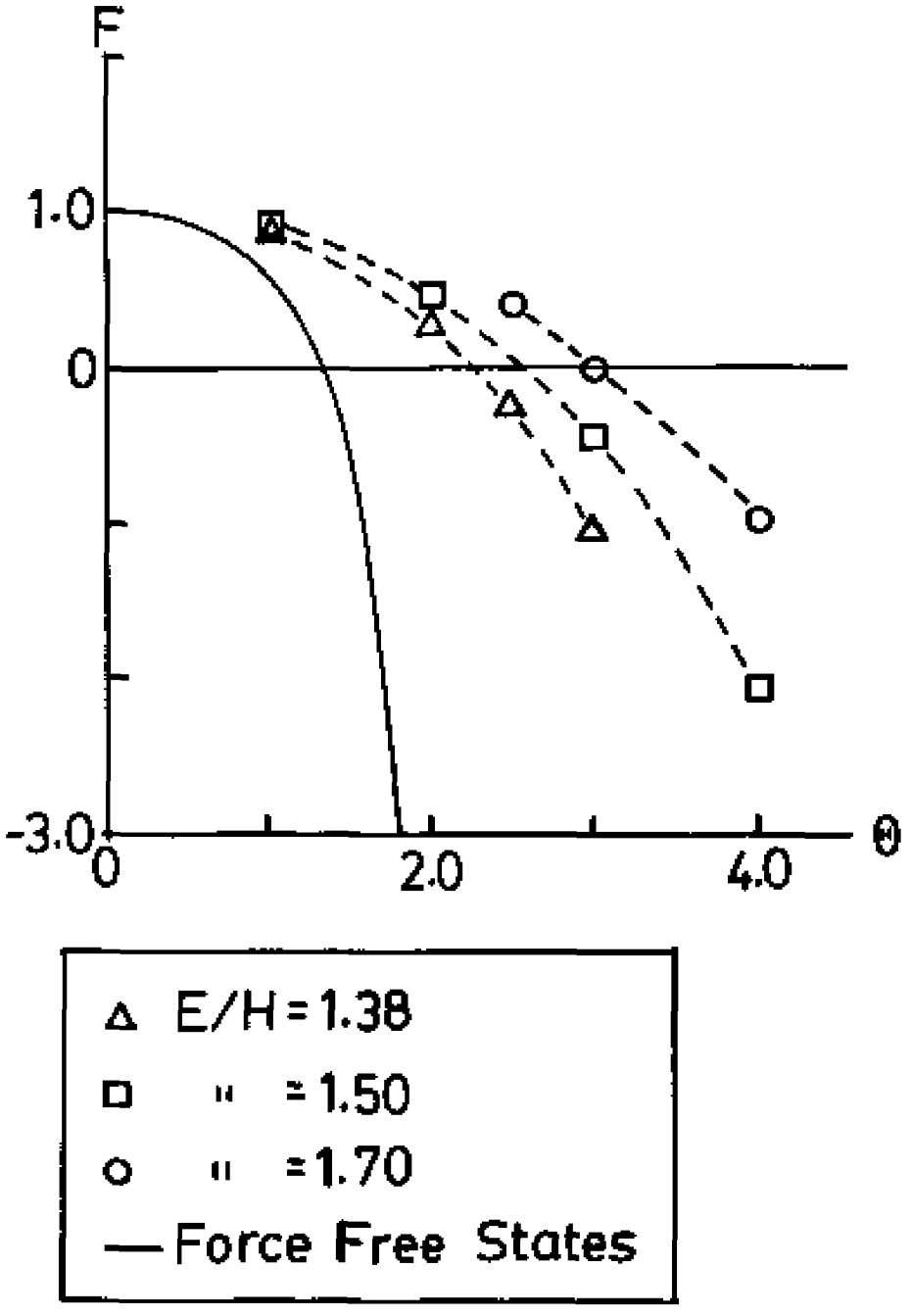

Fig. 23. F - Θ diagram for sequences of most probable reverse field pinch equilibria at different energy to helicity ratios.

discharge. Figure (23) is a diagram of F versus Θ for solution of the most probable state equations with various E/H. The solid curve represents the values of F and Θ which correspond to the analytic force-free solutions of Taylor's Bessel function model.[19] The values of E/H for these solutions are given in the legend of Fig. (23). One notices the tendency for increased reversal with increasing Θ for all cases. As E/H decreases, reversal occurs at progressively smaller values of Θ. In the present formulation of the most probable state equations, J_z is assumed to be non-negative, whereas the Bessel function force-free model demands that J_z be reversed when B_z is reversed, although such current profiles are not usually observed (this follows from $J_z(r) = \lambda B_z(r)$ in the Bessel function model). Therefore one cannot expect to find most probable reversed field equilibria which are force-free in this formulation.

As a final remark, it should be noted that reversed-field profiles with $\Theta = 2$ were found for sufficiently small E/H. However, no reversed field solutions were observed for $\Theta = 1.0$ despite an extensive search for such solutions within the $\beta - \gamma$ parameter space. This result is particularly interesting in light of predictions by Taylor[19] and others[18] which put the critical value of Θ for reversal in the range $1.2 \lesssim \Theta \lesssim 2.0$.

IV. REFERENCES

1. A. S. Bishop, Project Sherwood (Addison-Wesley, Reading, Mass., 1958.
2. A. Jeffry, T. Tanuiti, Magnetohydrodynamic Stability and Thermonuclear Containment (Academic Press, New York, 1966).
3. D. Montgomery, L. Turner, and G. Vahala, J. Plasma Phys. 21, 239 (1979).
4. F. Reif, Fundamentals of Statistical and Thermal Physics (McGraw-Hill, New York, 1965).
5. C. E. Shannon, The Mathematical Theory of Communication (University of Illinois Press, Urbana, 1949).
6. D. Montgomery, private communication.
7. G. Bateman, MHD Instabilities (The MIT Press, Cambridge, Mass., 1978).
8. T. G. Cowling, Magnetohydrodynamics (Adams Hilger Ltd., Longon, 1976).
9. H. Grad, AEC Report TID-7503,495 (1956).
10. G. F. Chew, M. L. Goldberger, F. E. Low, Proc. Roy. Soc. (London) A236:113 (1956).
11. H. Grad and H. Rubin, IAEA Geneva Conf., 31, 190 (1958).
12. V. D. Shafranov, in Reviews of Plasma Physics, edited by M. A. Lientovich (Consultants Bureau, New York, 1966) Vol. 2, p. 103.
13. J. D. Lawson, Proc. Phys. Soc. (London), B70, 6 (1957).
14. P. H. Sakanaka and J. P. Goedbloed, Phys. Fluids 17, 919 (1974).

15. M. D. Kruskal, J. L. Johnson, M. B. Gottlieb, Phys. Fluids, 1, 421 (1958).

16. M. Hagler, M. Kristiansen, An Introduction to Controlled Thermonuclear Fusion, D. C. Heath and Company, Lexington, Mass. (1977).

17. L. A. Artsimovich, Controlled Thermonuclear Reactions, Oliver and Boyd, Edinburgh (1961).

18. H. Bodin, in IIIrd Topical Conference on Pulsed High Beta Plasmas, D. E. Evans, Ed., Pergamon Press (1976).

19. J. B. Taylor, Proc. Vth IAEA Conference on Plasmas and Controlled Fusion, Paper CN 33/PD 1, Tokyo (1974).

20. A. Verhage, UKAEA Research Group Report CLM-R161, Culham Laboratory, Abingdon, Oxfordshire (1976).

21. W. F. Ames, Nonlinear Ordinary Differential Equations in Transport Processes (Academic Press, 1968).

22. K. M. Brown, SIAM Journal on Numerical Analysis, 6, 560 (1969).

23. International Mathematics and Statistics Library (IMSL), Houston, Texas.

24. D. Grove, et al., Proc. VIth IAEA Conference on Plasmas and Controlled Fusion, Paper CN 35/A 1, Vienna (1976).